

# NEW TECHNOLOGIES IN ELECTRON SPIN RESONANCE

---

Jack H. Freed

*Baker Laboratory of Chemistry and Chemical Biology, Cornell University, Ithaca,  
New York 14853; e-mail: jhf@ccmr.cornell.edu*

**Key Words** complex fluids, distance measurements, double quantum coherence, far-infrared spectroscopy, molecular dynamics, two-dimensional spectroscopy

■ **Abstract** New electron spin resonance (ESR) technologies have been developed, which have led to new and improved applications. (a) The development of two-dimensional Fourier transform (FT) ESR required spectrometers providing intense  $\pi/2$  microwave pulses of very short (3–5 ns) duration, wide bandwidths, and very short dead times. It has enabled studies that resolve sophisticated details of molecular dynamics in complex fluids. (b) Methods that produce multiple quantum coherences by pulsed ESR now enable accurate measurements of large distances ( $>12 \text{ \AA}$ ). (c) One of the most important advances has been the extension of ESR to high magnetic fields and high frequencies. This has benefited from the utilization of quasi-optical methods, especially above 150 GHz. The greatly improved orientational resolution and the faster “snapshot” of motions that are provided by ESR at high frequencies enhance studies of molecular dynamics. The use of both high and lower frequencies enables one to unravel faster and slower modes from the complex dynamics of fluids and macromolecules. (d) The development of FT-ESR imaging required substantial pulsed field gradients lasting only 50–100 ns. ESR imaging is effective in studying diffusion in fluids. Areas for further development are also described.

## INTRODUCTION

Electron spin resonance (ESR) (or electron paramagnetic resonance) has been experiencing a renaissance in the past 15 years, in some ways similar to that of nuclear magnetic resonance (NMR) (1) 1 or 2 decades earlier. Although most commercially produced spectrometers in use are still of the conventional cw design, albeit with such modern upgrades as computer control, and are operating at or near the X-band frequency of 9.5 GHz (with 35 GHz the next most popular), there have been major extensions, usually homemade, to much higher frequencies, to pulse and Fourier transform (FT) spectrometers, and to (low-frequency) ESR imagers. The instrumental challenges have been manifold, but new and improved applications of ESR are, we hope, even greater. It is my intention in this chapter to review the new

technologies, instrumental developments, their applications, and areas for further development. In this, I am largely motivated by applications of ESR to studies of molecular dynamics in fluids with chemical physical and biophysical applications, although I touch on other topics. Space limitations and personal interests further constrain this review. Previous related reviews have included those by Dalton et al (2) and by Stehlik & Möbius (3), as well as by Levanon & Möbius (4).

## PULSED ESR, TWO-DIMENSIONAL 2D-FT-ESR

### Overview

Let us first consider time-domain ESR, in particular pulsed ESR. Earliest developments date from Mims et al (5, 6), followed by the Novosibirsk groups (7, 8). Their focus was largely on solids, typically at low temperatures. Recent extensive developments in this regime have been provided by Schweiger and coworkers (9–11), Thomann & Bernardo (12), Hoffman et al (13), and many others (14–16). This is a regime of long relaxation times (often achieved by working at the lowest possible temperatures), making it possible to perform extensive pulse sequences in order to carry out one's objectives. However, the spectra generally have a very wide extent (especially in the case of transition-metal ions), so it is only possible to irradiate small portions at any one time, i.e. this is typically the regime of selective pulse sequences.

More challenging technological requirements are met in developing pulsed ESR for studies of dynamics in fluids. Here relaxation times are as low as nanoseconds for  $T_2$ s, but  $T_1$ s are often substantially longer (microseconds) for nitroxide spin labels. The challenges here are (a) to supply intense enough microwave radiation pulses that the electron spins can be rotated by angles of  $\pi/2$  in times short compared with  $T_2$ , and (b) to have spectrometer dead times short enough that signal decay due to  $T_2$  is not so great as to have completely quenched the signal after the dead time. As a by-product, it will be seen that short, intense pulses and short dead times are also the natural requirements for conducting FT experiments, wherein the whole spectrum is irradiated by a pulse of short duration, and one starts collecting either the free induction decay (FID) or the echo decay as soon after the pulse(s) as possible. Once the FID is collected, then it becomes possible to perform two-dimensional (2D)-FT ESR experiments (cf Figure 1), by analogy to 2D-NMR.

### Early FT-ESR

Hornak & Freed (17) analyzed the challenge of performing FT-ESR, and they provided an experimental demonstration using a semiquinone with a spectral extent of ca 20 MHz. An earlier example of an FID in the liquid state was provided by Eliav & Freed (18), who distinguished between a transient photoelectron and a solvated electron by their different FT spectra. Another example was provided

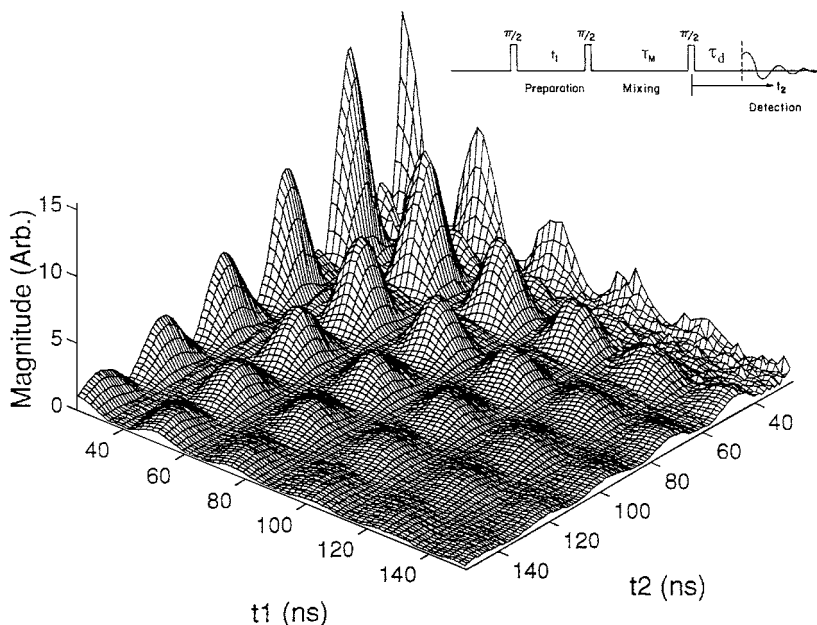


**Figure 1** Two-dimensional electron double resonance (ELDOR) at 17.3 GHz. The time domain  $S_{c-}$  spectrum showing ESR timescale; from phospholipid that is end chain labeled with nitroxide (16-PC) in lipid vesicles (46). (*Inset*) Pulse sequence.

by Lebedev and coworkers (19). These latter observations could be obtained with older conventional ESR techniques. That is, given the limited spectral extent of ca  $\pm 10$  MHz, long  $\pi/2$  pulses of ca 25–30 ns, a rotating  $B_1$  of (3 G) could be used, and with  $T_2$ s greater than 1  $\mu$ s, 150- to 200-ns dead times could be tolerated. In addition, a conventional box-car integrator was used to separately collect each point of the FID. [Also, this “older” technology could be used to perform 2D–electron-spin-echo experiments on very viscous fluids, where one steps the magnetic field using selective pulses (20, 20a).] This contrasts with the new technology, which was directed to spectral extents of ca  $\pm 50$  MHz,  $T_2$ s of several hundred nanoseconds, and an averaging transient digitizer that provided effective 1- to 5-ns time stepping, to collect many points along each FID.

## Development of 2D–FT-ESR

The “modern era” of pulsed ESR in fluids started in 1986 when Gorcester & Freed (21) and Gorcester et al (22) obtained the first 2D–FT-ESR experiments collecting either the FID or the echo decay on nitroxides in liquid solutions in the fast motional regime with pulse widths of 15 ns. At about this time, others (23–25) were collecting FIDs of organic radicals with spectral extents of ca  $\pm 10$ –25 MHz and  $T_2$ s of microseconds. Further improvements, including extensive use of phase-cycling

sequences to cancel instrumental imperfections and unwanted coherence pathways, permitted a quantitative study on Heisenberg spin exchange (HE) (26). Unlike cw studies, where concentration-dependent measurements are required to extract the HE rates, a single 2D-exchange experiment is sufficient for its determination. Angerhofer et al (27) then showed how this approach applied to chemical exchange. In a further study, Gorcester et al (28) showed how rotational dynamics could be effectively studied in a liquid crystal containing a nitroxide probe by a combination of 2D-exchange (now called 2D-ELDOR, for 2D electron spin–double resonance) (cf Figure 1) and 2D spin-echo experiments. They enabled one to separate the three relevant spectral densities— $j_{DD}(0)$ ,  $j_{DG}(0)$ , and  $j_{DD}(\omega_n)$ —arising from dipolar and g-tensor interactions, which could not be achieved by conventional cw line-width measurements. In addition, inhomogeneous line-width contributions (a significant problem, especially with oriented samples) are cancelled out in the spin-echo experiments but not in cw experiments. This enabled a more accurate assessment of relevant motional models. Miick & Millhauser (28a) have shown how 2D-ELDOR effectively delivers HE rates for spin-labeled peptides in aqueous solution.

What remained was the challenge of performing 2D-ELDOR and COSY (correlation spectroscopy) experiments over the whole motional range: fast motional to slow motional to the rigid limit, using nitroxide spin probes. Here the challenges were generating very short (and intense)  $\pi/2$  pulses of 5 ns or less to irradiate spectra that are 220 MHz wide, and to have this wide a bandwidth in the resonator. The solution proved to be the use of a special loop gap resonator with very low Q (ca 40–50) and a large filling factor (29, 30). Froncisz & Hyde (31) had extensively developed the loop gap resonator largely for cw-ESR; Hornak & Freed (32) had pointed out its virtues for pulsed ESR; Pfenninger et al (33) had developed a useful variant, a bridged loop gap resonator. Patyal et al (29) were able to adapt the design to provide the wide bandwidths. Their work indicated the value of the ESR-SECSY (spin-echo correlation spectroscopy) and 2D-ELDOR experiments in the slow-motional regime. It was, however, found that reduced dead times, better spectral coverage, and better spectrometer performance were required to avoid spurious signals resulting from, for example, pulse interactions before quantitative studies could be performed. In addition, a slow-motional theory for these experiments was required.

## Complex Fluids Studied by 2D-ELDOR

Once such improvements were made, it became possible to perform detailed studies on complex fluids (34, 35). These included phospholipid membrane vesicles (cf Figure 1) (34, 35), liquid crystalline solutions (36, 37), and liquid crystalline polymers (38). A key feature was dead times of ca 50–60 ns. A detailed theory of 2D-FT-ESR in the slow motional regime was provided by Lee et al (39), which enabled quantitative analysis of these 2D spectra. In the case of 2D-ELDOR, simultaneous fits of experiments at several mixing times,  $T_m$ , provided, in effect, a third dimension. One could watch how the cross peaks grow in relative to the

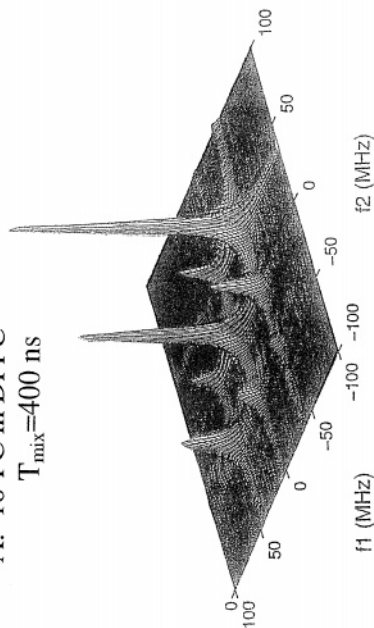
auto peaks with increasing mixing time, (cf Figures 2 and 3). This supplies quantitative information on the nuclear-spin-flip-inducing processes of both HE, which reports on translational diffusion, and the intramolecular electron-nuclear dipolar interaction, which reports on the tumbling motions.

In addition, the line shapes of the auto and cross peaks are particularly informative. In fact, there are two types of line shapes provided by the COSY and 2D-ELDOR experiments. They arise because the experiment provides two types of 2D spectrum, depending on the coherence pathway: One is FID-like (sometimes referred to as the anti-echo) and the other is echo-like, i.e. there is a refocusing of the inhomogeneous broadening (IB) terms in the spin-Hamiltonian leading to their cancellation in the echo formation. The echo-like (or  $S_{c-}$ ) 2D signal can in fact be transformed to provide just the homogeneous broadening (HB) along one frequency dimension,  $\omega_1$ , whereas the other frequency dimension,  $\omega_2$ , provides essentially the cw spectrum. This transformation takes one from the COSY to the SECSY format. In the 2D-ELDOR spectrum, this same transformation will yield the HB for the auto peaks, but the cross peaks will be affected by any differences in the IB existing between the two spectral lines connected by that cross peak. Thus, the 2D-ELDOR  $S_{c-}$  spectrum provides detailed information on spin relaxation via the cross-peak development and the HB of the auto peaks, whereas the differences in IB show up in the cross peaks. The FID-like  $S_{c+}$  2D spectra include the full effects of inhomogeneous broadening. The 2D-SECSY format is particularly useful for ultraslow motions, for example macromolecules in viscous media (39a).

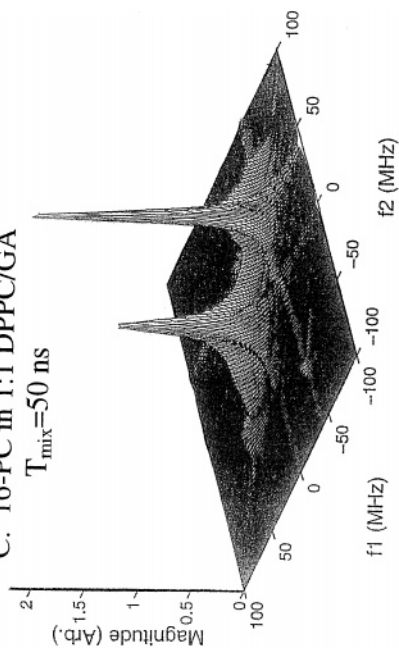
**Membrane Vesicles** Lee et al (39) showed that taken together, the  $S_{c-}$  and  $S_{c+}$  2D-ELDOR spectra are especially useful for the study of the dynamics and structure of complex fluids. This is because complex fluids typically show a microscopic structure, such that molecular tumbling occurs with respect to this structure, which provides the local orientational alignment. This can be readily appreciated in the case of lipid membranes. If they are macroscopically aligned, then one would observe the different “single-crystal-like” spectra obtained for each orientation of the membrane normal with respect to the constant magnetic field. Membrane vesicles, however, simultaneously have membrane components at all angles with respect to the magnetic field, and they thereby provide “powder-like” spectra. The extent of the local ordering is thus reflected in the IB, and details about the aligning fields can be obtained from the differences of the IB for the different hyperfine (hf) lines. At the same time, the  $S_{c-}$  spectra permit one to obtain dynamics from the homogeneous  $T_{2s}$  and the development of the cross peaks with mixing time. Such a program was carried out by Patyal et al (34, 35) using several different nitroxide spin labels in phospholipid membrane vesicles to obtain accurate dynamic and ordering parameters.

In general, one finds that the 2D-ELDOR spectra from membrane vesicles show more dramatic changes as the membrane properties are varied. This can even enable simple interpretations of these spectra just in terms of pattern recognition. For example, in Figure 3, 2D-ELDOR contour plots as a function of mixing time,

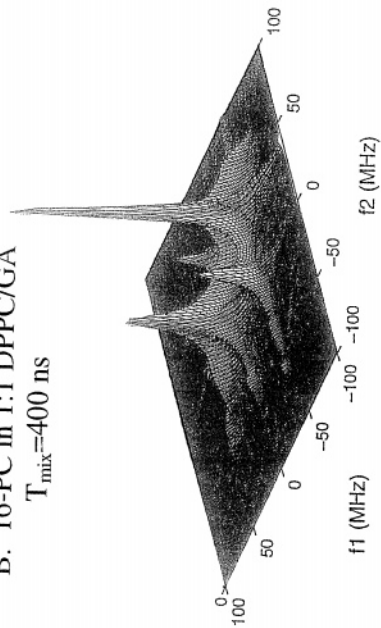
A. 16-PC in DPPC  
 $T_{\text{mix}}=400$  ns



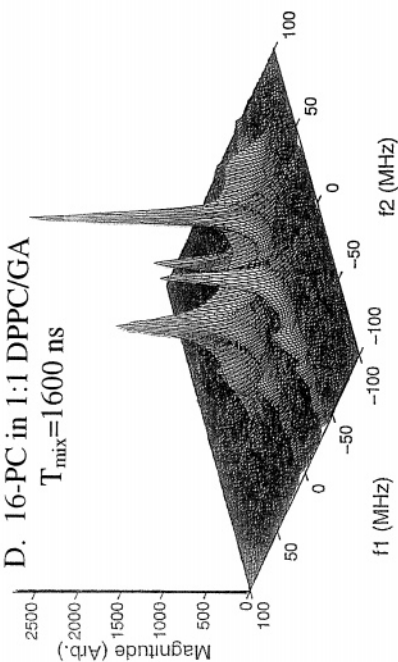
C. 16-PC in 1:1 DPPC/GA  
 $T_{\text{mix}}=50$  ns



B. 16-PC in 1:1 DPPC/GA  
 $T_{\text{mix}}=400$  ns



D. 16-PC in 1:1 DPPC/GA  
 $T_{\text{mix}}=1600$  ns



$T_m$ , are shown for the spin-labeled lipid, 1-palmitoyl-2-(16-doxyl stearoyl)phosphatidylcholine (16-PC) in pure lipid vesicles and for a lipid-cholesterol mixture in the ratio 1:1. The former is in the standard liquid crystalline phase, whereas the latter is in a “liquid-ordered” (LO) phase (40). The spectra are qualitatively different, emphasizing that the LO phase exhibits significantly greater ordering than the liquid crystalline phase at 51°C. The increased microscopic ordering leads to increased IB affecting the spectra from the LO phase. In addition, the restriction of the range of orientational motion, due to the microscopic ordering in the LO phase, shows up as a much slower development of cross peaks vs  $T_m$ .

**The Slowly Relaxing Local Structure Model** In addition to the microscopic ordering but macroscopic disorder (MOMD) (41) that gives rise to complex inhomogeneous line shapes, these spectra are often in the slow-motional regime, i.e. the motions are too slow to provide complete averaging of the rigid-limit line shapes. This is another source of IB that is effectively dealt with in the theory of Lee et al (39). The large inhomogeneities one obtains mean that the  $S_{c+}$  spectra often decay during the 50- to 60-ns dead times to unobservable levels, and only the  $S_{c-}$  spectra, with their substantial cancellation of IB, can be observed. On the other hand, these slow motional spectra provide more insight into the microscopic details of the molecular dynamics because their timescales are comparable. It was found that for complex fluids, a more sophisticated model than the MOMD model was needed to analyze the 2D-FT-ESR spectra in order to achieve reasonably good agreement with experiment. The precise model that has been utilized is known as the slowly relaxing local structure (SRLS) model (42–44). It differs from the MOMD model in that the local structure sensed by the reorienting spin-probe (or spin-label) is itself allowed to relax, but on a longer timescale. This more sophisticated model involves additional parameters to be fit: viz the relaxation rates of the anisotropic potential characterizing the structure (or cage) around the spin probe (44), as well as the orientation of the symmetry axes for this structural relaxation relative to the symmetry axes for its aligning potential (45).

**Oriented Liquid Crystals** Sastry et al (36, 37) used studies on the macroscopically aligned liquid crystal solvent 4O,8 (butoxy benzylidene octylaniline) to test the applicability of the SRLS model. This is a liquid crystal that exhibits many phases as a function of temperature, including isotropic, nematic, liquid-like smectic A, solid-like smectic B, and crystalline phases. They found consistently better fits using a SRLS model (in addition to the macroscopic liquid crystalline orienting potential) than with the standard simpler model that does not include any local

←  
**Figure 2** Two-dimensional electron double resonance (ELDOR) at 17.3 GHz showing effect of peptide gramicidin A (GA) on dynamic structure of lipid membrane containing (end chain) nitroxide labeled lipid (16-PC) at 75°C. (A) Pure lipid, mixing time,  $T_m = 400$  ns. (B, C, D) 1:1 lipid to GA with  $T_m = 400$  ns, 50 ns, and 1.6  $\mu$ s, respectively (56). DPPC, dipalmitoyl phosphatidylcholine.

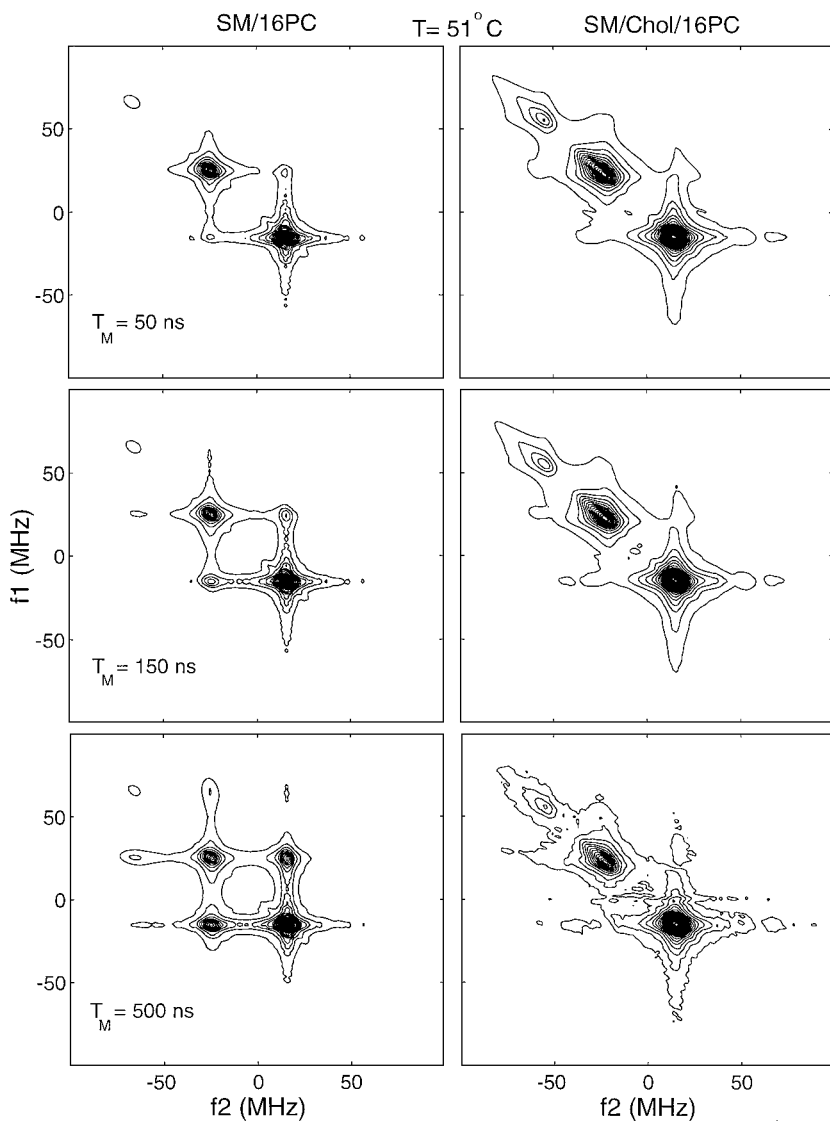


**Figure 3** Two-dimensional electron double resonance at 17.3 GHz vs mixing time,  $T_m$ , of 16-PC in liquid crystalline phase from pure lipid vesicles (*left side*) compared with 16 PC in liquid-ordered phase from 1:1 ratio lipid to cholesterol (*right side*) at 50°C.

structure. In general, the cage potential is of the order of  $kT$  (where  $k$  is Boltzmann's constant and  $T$  is temperature) to several times  $kT$ . An interesting observation was made with the large rigid cholesterol-like nitroxide (CSL) probe (36). It was found that at the  $S_A \rightarrow S_B$  transition (i.e. the transition from the liquid-like to solid-like smectic phase), the local structure potential drops significantly, whereas the macroscopic aligning potential increases by almost the same value. This indicates that most of the local structure "freezes out," and thereby contributes to the macroscopic alignment. The results with a small nitroxide probe, perdeuterated tempone (PDT) (37), show more clearly an effect previously inferred from cw-ESR. The PDT is gradually expelled from the more highly ordered hard-core region toward the more flexible aliphatic chain region as the temperature is lowered, as a result of increased core packing from the smectic layer formation, and it thus experiences a fluid local cage structure even as the temperature is reduced. In another 2D-FT-ESR study on a liquid crystalline polymer, the SRLS model was effective for the results in the fluid phase, whereas the MOMD model was sufficient in the solid phase (38). [An earlier version of pulsed ELDOR using selective pulses, known as field-stepped electron-spin-echo ELDOR (20a), has been used by Spiess and coworkers (45a) in a 2D format to study polymers in the solid state at low temperatures.]

These studies, in aligned liquid crystal solvent, demonstrated the very extensive relaxation, dynamic, and structural information that one can obtain from 2D-ELDOR experiments performed as a function of mixing time. In all, 10 such parameters could be effectively extracted. They include the two-term (asymmetric) macroscopic orienting potential in the liquid crystalline phases, the axially symmetric diffusion tensor for the probe, its two-term orienting potential in the local structure or cage, the relaxation rate for the cage, the residual homogeneous  $T_2^{-1}$  due to processes other than the reorientational modulation of the  $^{14}\text{N}$  dipolar and  $g$ -tensors, the residual (Gaussian) inhomogeneous broadening not due to the specific slow-motional contributions from the  $^{14}\text{N}$  hf and  $g$ -tensors, and the overall  $T_1$  for the electron-spins. (The concentration was kept low enough that the HE rate was negligible.) These constitute virtually all the parameters that one can hope to obtain from any ESR experiment(s) on spin relaxation in a complex fluid!

## Recent Technical Development

**Signal-to-Noise Ratio and Frequency Dependence** Further improvements in modern pulsed ESR techniques clearly required (a) reduced dead times, (b) more intense and shorter  $\pi/2$  pulses, and (c) increased signal-to-noise ratio (SNR). A successful effort was made to address these issues by Borbat et al (46), who extended 2D-FT-ESR techniques to 17.3 GHz (Ku band). One generally expects to achieve improved sensitivity by going to higher frequencies. Borbat et al have analyzed this for FT-ESR spectroscopy (46). For the case of keeping the resonator filling factor and the spectral bandwidth constant, they find that  $N_{\min} \propto \omega^{-7/2}$ , but  $(N/V_s)_{\min} \propto \omega^{-1/2}$ , where  $N_{\min}$  is the minimum number of spins,  $\omega$  is the (angular) frequency, and  $V_s$  is the sample volume. Further details may be found elsewhere (46).

Thus we see that by going to higher frequencies, it should be possible to significantly improve sensitivity and/or spectral coverage. [Additional discussion of frequency dependence of sensitivity may be found elsewhere (47).]

**Dead Time** The dead time is arguably the most important feature of a fast-pulsed ESR spectrometer (46). That is, the signal after the dead time,  $\tau_d$ , for FID detection is  $S \propto N \exp[-\tau_d/T_2^*]$ , where  $T_2^*$  is the FID time constant. For echo detection, it is  $S \propto N \exp[-2\tau_d/T_2]$ , with just the homogeneous  $T_2$  affecting the decay. Thus a large  $\tau_d$  has more serious implications for the SNR than a reduced  $N$ . Borbat et al describe the key factors that affect  $\tau_d$  and how they succeeded in reducing  $\tau_d$  to 25–35 ns (46). They suggest that use of a bimodal resonator (48), which provides good (ca 30–40 dB) isolation between the irradiating and detecting arms of the bridge, could reduce  $\tau_d$  to as short as 10–15 ns. Additional improvements might be achievable by the use of a bucking circuit designed to partially cancel the pulse signal before it reaches the detector (49).

**Intense Pulses** We now consider the challenge of more intense pulsed  $B_1$  fields to allow for shorter pulses that provide greater spectral coverage. So far, the best conditions that have been achieved yield about 30 G for  $B_1$  in the rotating frame corresponding to 3.2-ns  $\pi/2$  pulses when using a 2-kW power source and a small dielectric ring resonator at 17.3 GHz ( $6.5 \times 2.8 \times 5$  mm). One may increase the  $B_1$  fields by using even smaller resonators at the expense of sample size. Alternatively higher-power TWT amplifiers (e.g. 10 kW) could be used. Specially tailored composite pulsing is a way to improve coverage without actually increasing  $B_1$  (50). Another approach would be based upon a pulse compression method (51). In nearly all cases, 2D-FT-ESR spectra require extensive phase corrections to obtain pure absorption. Procedures for motionally narrowed spectra have been described by Gorcester & Freed (26, 52) and Gorcester et al (53) and for slow-motional spectra by Saxena & Freed (54). In the past, extensive use was made of magnitude spectra, which require no phase corrections, at the expense of spectral resolution (54).

**Multifrequency Pulse Spectrometer** The state-of-the-art pulsed 9.3/17.3 GHz 2D-FT-ESR spectrometer of Borbat et al (46) has a sensitivity at 17.3 GHz, corresponding to a minimum number of detectable spins ( $\text{SNR} = 1$ ) of  $6 \times 10^{13}$  spins/s<sup>1/2</sup> for a 2D experiment, which is close to their theoretical estimate of  $2 \times 10^{13}$  spins/s<sup>1/2</sup>. This was achieved with 5-ns  $\pi/2$  pulses, a  $Q_L = 90$ , and a 10-kHz repetition rate. They could obtain very good 2D spectra ( $\text{SNR} \sim 4000$ ) in 20 min using 10 nmol of spin probe. This means good signals ( $\text{SNR} \sim 200$ ) could be achieved with 0.5 nmol of spin probe, or about 150 pmol in 3 h. of data acquisition. They estimated that a signal digitizer faster than theirs (which was at 200 Msps), as well as repetition rates greater than 10 kHz, could reduce the minimum number of spins by a factor of 5. Also, they found that the concentration sensitivity at Ku band was four to eight times better than they could achieve at X band.

## Meeting the Challenge: Lipid-Peptide Interactions

The virtues of the improved 2D-FT-ESR technology were well demonstrated in studies of the effect of the peptide, gramicidin A (GA), on the dynamic structure of model membranes. Patyal et al (55) clearly showed by 2D-ELDOR that the principal effect of adding GA to the liquid and crystalline phase was to decrease both the rotational and translational rates of the end chain-labeled lipids, with no significant change in the local ordering. The changes in the 2D-ELDOR spectra on adding GA were much more dramatic than the changes in the cw-ESR spectra, clearly emphasizing the much greater sensitivity of the former to molecular dynamics. However, these studies, performed at 9.3 GHz with a  $\tau_d$  of 50–60 ns, related just to the bulk lipids. They showed no clear indications of the so-called boundary lipids that coat the peptide. Evidence for the boundary lipid exists in cw-ESR spectra but is of very limited resolution. Patyal et al argued that its absence in their 2D-ELDOR experiments was due to the fact that its homogeneous  $T_2$  is too short to permit it to be seen after a spin-echo dead time,  $2\tau_d \sim 100$ – $120$  ns. This implied that it is in the slow motional regime (but not yet close to the rigid limit). More recently Borbat et al (56), using 17.3-GHz 2D-ELDOR with its increased SNR and decreased dead times ( $2\tau_d \sim 50$ – $60$  ns), have been able to obtain 2D-ELDOR spectra that clearly show the presence of two components, viz the bulk lipid component, previously seen by Patyal et al (55), which shows relatively fast dynamics, and a second, the presumed boundary lipid, which grows in as GA is added (cf Figure 2). Its 2D-ELDOR spectrum is clearly that of a more slowly reorienting lipid, as expected. However, even at these short dead times, it was found that the low-frequency hf-component auto peak and its associated cross peaks were difficult to see above the noise level (even for the sharper bulk lipid spectrum) because its  $T_2 \leq 10$  ns is very short. In addition, simulations of these spectra show that additional rapidly relaxing features of the bulk and boundary lipid spectra have decayed away. These important spectral sources of information would require even shorter dead times,  $2\tau_d < 20$ – $30$  ns.

Additional 2D-FT-ESR studies on fluids have been performed (57–60). Other time-domain techniques for fluids include time-resolved ESR, which has been used extensively for electron-spin polarization (CIDEP) studies (61–64) and saturation recovery (65–67).

## MULTIPLE-QUANTUM ESR: DISTANCE MEASUREMENTS

### Overview: Double Quantum Coherence

The determination of distances within and between molecules has become an important application of ESR, with its many aspects summarized in a new monograph (68). Here we emphasize what is the newest, and probably one of the most powerful for measuring longer distances,  $> 12$  Å. It is based upon double quantum

coherence (DQC) pulsed ESR methods, which have only been developed in the past few years (69–72). [Here multiple quantum refers to interacting spins, as in NMR. Hyde and coworkers (73) have developed a very different multiple quantum ESR technique, which involves the absorption/emission of many photons or radiation quanta in a cw saturation experiment.]

Basic electron-spin-echo (ESE) methods had been extensively applied in the 1970s and 1980s to study distances as well as distributions of spins (7, 8, 74). To overcome several of the weaknesses of these ESR methods, two improved ESE techniques were introduced: double electron-electron resonance (DEER or PELDOR) (75, 76) and 2 + 1 ESE (77, 78) that use selective pulses (although the 2 + 1 technique would be consistent with nonselective pulses).

Initially, Saxena & Freed (69) were able to obtain DQC signals from a bilabeled synthetic peptide at 9.3 GHz using a sequence of five pulses of about 15–17 G. They did not correspond to standard DQC pathways, and these workers ascribed their observation to a “forbidden” coherence pathway that arises from the fact that  $\gamma_e B_1$  is not much greater than  $d$ , the dipolar interaction between the two nitroxide spin labels following an analogous case in NMR (79). They then carried out rigorous numerical calculations (70), which enabled them to calculate this signal and to assign a distance of ca 20 Å between the labeled ends of the peptide, in agreement with their preliminary assessment. But this experiment suffered from weak signals and difficulty in the precise adjustment of the  $B_1$  field to its optimum value.

## Pulse Sequences

With the shorter dead times and shorter  $\pi/2$  pulses of the Borbat et al pulse spectrometer operating at 17.3 GHz (46), Borbat & Freed (71, 72) were able to achieve strong allowed DQC signals that were comparable to standard single quantum (SQ) signals, and they could be obtained routinely in a variety of bilabeled nitroxide systems in both disordered and oriented solids. They introduced three different pulse sequences. Their four-pulse sequence involves a first  $\pi/2$  pulse that converts the spins at equilibrium into SQ coherence (SQC), represented by spin operators  $S_{1y}$  and  $S_{2y}$ , which evolves during preparation time  $t_p$  under the effects of the dipolar interaction into antiphase SQC (represented by spin operators  $S_{1x}S_{2z}$ ,  $S_{1y}S_{2z}$ , and those obtained by permuting spin indices 1 and 2). The second  $\pi/2$  pulse produces the DQC ( $S_{1x}S_{2y} + S_{1y}S_{2x}$ ), which evolves during a period  $2t_1$ , with a refocusing  $\pi$  pulse placed at the middle of this period. The third  $\pi/2$  pulse converts the DQC back into anti-phase SQC, which then evolves during time  $t_2$  into observable SQC ( $S_{1y}$  and  $S_{2y}$ ), forming an echo at  $t_2 = t_p$ . One collects the echo envelope as a function of  $t_p$ . Extensive phase cycling is utilized to select only this coherence pathway from the many others that are created by this pulse sequence.

The theoretically most desirable pulse sequence utilized by Borbat & Freed (71, 72) is the six-pulse sequence:  $\pi/2-t_p-\pi-t_p-\pi/2-t_1-\pi-t_1-\pi/2-(t_m-t_p)-\pi-(t_m-t_p)$ -echo. The inclusion of the three  $\pi$  pulses refocuses the coherences at

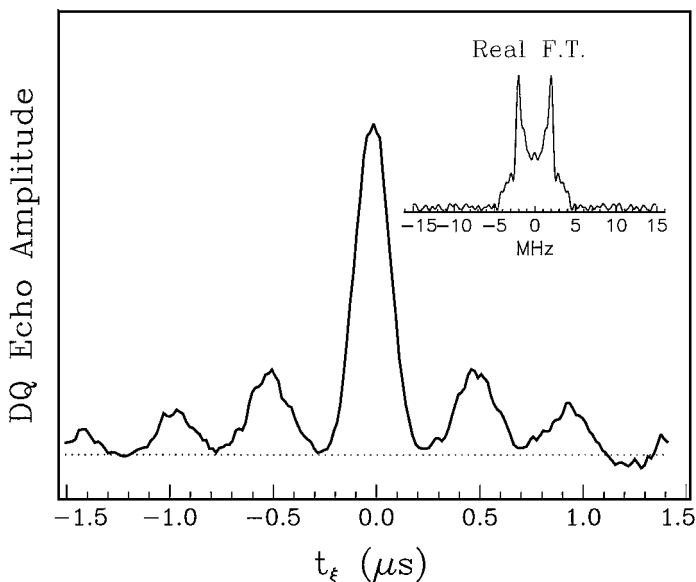


**Figure 4** Six-pulse double quantum (DQ) coherence time domain signal, from rigid organic radical that is nitroxide labeled at both ends in frozen solution at  $-62^{\circ}\text{C}$ , showing dipolar modulation. It yields the distance between nitroxides of  $28.8 \pm 0.5 \text{ \AA}$ . (*Inset*) Pake pattern obtained by Fourier transforming (F.T.) time domain signal (72).

each stage. This sequence is used with constant  $t_m$ , whereas  $t_p$  is varied. The echo envelope is recorded as a function of  $t_{\xi} \equiv t_m - 2t_p$ , which has a range of  $(-t_m, t_m)$ . This sequence is thus virtually “dead-time free”, and it eliminates any  $T_2$  relaxation decay vs  $t_{\xi}$  (cf Figure 4). Their approximate theory provides the following:

$$V_{6,DQ}(\Delta\Omega_1, \Delta\Omega_2, r, t_p) = \bar{V}_{6,DQ}(\Delta\Omega_1, \Delta\Omega_2) \sin(at_p) \sin[a(t_m - t_p)]$$

$$\xrightarrow{B_1 \rightarrow \infty} -\sin(at_p) \sin[a(t_m - t_p)] = -\frac{1}{2} [\cos at_{\xi} - \cos at_m].$$

where  $a = d + 2J$  with the dipolar interaction  $d = \gamma_e^2 \eta (1 - 3 \cos^2 \theta) / r^3$  and exchange interaction  $J$  for a radical pair separated by a distance  $r$  with  $\theta$  the angle between  $r$  and the direction of the static magnetic field. Here  $\Delta\Omega_1$  and  $\Delta\Omega_2$  represent the resonance frequency offsets of electron spins 1 and 2. The function  $\bar{V}_6(\Delta\Omega, \Delta\Omega_2)$  is a measure of the extent of coverage by the microwave radiation, i.e. it depends on  $|\Delta\Omega_1 / \gamma_e B_1|$  and  $|\Delta\Omega_2 / \gamma_e B_1|$ .  $\Delta\Omega_1$  and  $\Delta\Omega_2$  depend on the orientations of the dipolar and g-tensors for nitroxides 1 and 2, respectively, on the molecule, and in general they can be correlated with their  $r$  vector. This can significantly complicate the analysis when one integrates over all the molecules, especially because such correlations are not known a priori. A

simple case exists when they are not correlated. Then one can separately average the term in  $\sin(atp) \sin[a(t_m - t_p)]$ . An even more favorable case is the limit of nonselective pulses (i.e.  $B_1 \rightarrow \infty$ ) wherein  $V_{6DQ}(\Delta\Omega, \Delta\Omega_2, r, t_p) \rightarrow -1/2[\cos at_\zeta - \cos at_m]$ , and the signal becomes independent of any resonance offsets. Integration of this function over  $\theta$ , as appropriate for a disordered solid, followed by an FT, yields the classic Pake doublet pattern from which the value of  $1/r^3$  is readily extracted. In particular, shoulders in the Pake doublet are seen that correspond to the canonical  $\theta = 0$  and  $\pi/2$  orientations, (cf Figure 4). Borbat & Freed (71, 72) also show Pake doublets for oriented samples such that  $\theta = 0$  or  $\pi/2$ .

In the case of spectra of limited spectral width (ca 5 G), Borbat & Freed (71) achieved the  $B_1 \rightarrow \infty$  limit. However, their use of  $B_1 \approx 30$  G precluded reaching this limit for the nitroxide biradicals. As is well-known,  $\pi$ -pulses require twice the  $B_1$  as  $\pi/2$ -pulses in order to have the same pulse width and thereby to achieve the same bandwidth. Instead they had to use  $\pi$ -pulses of approximately twice the pulse width (i.e. 6.2 ns), which reduced spectral coverage, leading to some signal attenuation.

Thus, we find two reasons why it would be desirable to increase  $B_1$  for these DQC experiments: (a) Better coverage would provide a better SNR because a greater fraction of the spins will be properly irradiated, and (b) it would reduce the need for corrections in the analysis arising from correlations between coverage factors and the orientation of the  $r$  vector. Estimates show that for nitroxides,  $B_1 \sim 60$  G would significantly improve both matters compared with the  $B_1 \sim 30$  G that was used (72).

## Advantages of DQC in Distance Measurements

The main advantages of this DQC method compared with the excellent DEER method developed by Tsvetkov's group (76) are as follows: (a) Signals are significantly stronger because DEER requires selective pulses that irradiate only small fractions of spins, which results in (b) lower-concentration samples that can be studied, which is important for biological samples; and (c) it is possible to suppress the effects of correlations between coverage factors and  $r$  in the DQC, but this is not the case for DEER (72). DEER, on the other hand, does not have any interferences from electron-spin-echo envelope modulation (ESEEM) because it is an incoherent method, but Borbat & Freed do find they can suppress the ESEEM in the DQC experiment, and/or the ESEEM oscillations occur at markedly different frequencies than the dipolar-induced DQC oscillations. DQC can be successfully performed with smaller  $B_1$  fields, and it does not require two microwave frequencies as does DEER (76, 80).

Finally, the techniques introduced by Borbat & Freed for DQC and zero quantum coherence can be adapted to generate higher-order coherences, again by analogy to NMR (1). This would enable the study of several interacting spin-labeled systems (e.g. protein or polymer aggregates), a potentially valuable application. These

experiments would benefit from the development of accurate, digitally controlled phase shifters that could provide a wide range of phase shifts as needed to filter the different coherence orders. Additionally, the development of pulsed field gradients (cf section on ESR imaging) of 10–100 G/cm, which can be switched on and off in several nanoseconds in order to cancel unwanted coherences (as is done in NMR), would enable one to simplify the phase cycling.

All in all, these DQC experiments, with their sophisticated pulse sequences and their filtering of just the desired coherence pathways, clearly demonstrate that with rapid current development of pulsed microwave instrumentation, pulsed ESR is now poised to exploit many sophisticated pulse methods developed in NMR that are based upon the ability to perform (nearly) nonselective  $\pi/2$  and  $\pi$  pulses. It still remains a challenge to carry these sequences out at or near room temperature, where  $T_2$  remains short.

## HIGH-FIELD/HIGH-FREQUENCY ESR

### Overview

One of the most important instrumental advances has been the extension of ESR to high magnetic fields and high frequencies (HFHF) corresponding to the millimeter-wave region. Although there had been previous use of far-infrared (FIR) spectroscopy that included applied magnetic fields in solid state physics (81–83), modern HFHF ESR with high SNR and high spectral (and magnetic field) resolution was introduced by the research group of Lebedev in Moscow (84, 85). Their 150-GHz spectrometer (operating at 5.4 T) corresponding to 2-mm wavelength involved sophisticated application of microwave technology (e.g. waveguides and cavity resonators). This pioneering tour de force took high-sensitivity, high-resolution ESR to the maximum frequency at which microwave technology could sensibly be used. Many useful applications of HFHF ESR were presented by Lebedev and his group during the 1980s (85).

### Quasi-Optics

The question remained how to take high-resolution ESR to higher fields and frequencies. Freed and coworkers showed that the answer lay with the use of millimeter-wave quasi-optical technology, when they reported on a 9-T, 250-GHz (i.e. 1.2 mm) HFHF ESR spectrometer (86, 87). This is in the “near-millimeter” range (i.e. wavelengths of 2–0.1 mm), which corresponds to the long wavelength end of the FIR regime. [The Grenoble group were meanwhile extending the simpler solid state type of FIR technique, referred to above, to the higher magnetic fields (88).] Quasi-optics refers to the fact that at FIR frequencies, one uses techniques that are a natural extension downward in frequency from optical techniques. Quasi-optics thus applies when a geometrical optics description, valid at visible wavelengths, no longer applies. Geometrical optics corresponds to a ray

description of radiation that ignores its wave-like properties (e.g. point focus and nondiffracting beams). In the FIR, where wavelengths  $\sim 1$  mm, and with optical structures having linear dimensions of a few centimeters, geometrical optics is no longer valid. In fact, diffraction plays a crucial role in the system behavior. This is described, to a good approximation, by Gaussian beams, which are modified plane waves whose amplitude decreases as one moves radially away from the optical axis (89, 90). The simplest, or fundamental, Gaussian beam has an  $\exp(-\rho^2/w^2)$  radial dependence, where  $\rho$  is the radial distance from the optical axis and  $w$  is the position-dependent  $1/e$  radius of the electromagnetic field (90). The phase of a Gaussian beam also differs from that of a plane wave due to diffraction effects.

## Quasi-Optical Transmission Spectrometer

The original 250-GHz ESR spectrometer of the Freed group is a transmission mode design, wherein a quasi-optical lens train was used to propagate the beam from source to Fabry-Perot (FP) resonator and then on to the detector (86, 87). The quasi-optical lens train mainly consisted of a series of longer (4.5 inch) focal length primary lenses that refocus the diverging beam and thereby propagate the beam over substantial distances. This method of propagation is much more efficient than that of waveguides; the loss incurred by the lenses over a 54-inch path length is only 2 dB, whereas the theoretical loss of WR-4 waveguide over the same distance is 16 dB. Also, quasi-optical feed horns in conjunction with focusing lenses are used to launch the linearly polarized beam from the source and to collect the beam into the detector. Similarly, the radiation is coupled into and out of the FP resonator with two conical feed horn/focusing lens pairs. The FP resonator was semi-confocal (to permit placing a sample on the flat bottom mirror) with a mode number,  $\nu = 20$  (i.e. approximately the number of half-wavelengths between the mirrors), and provided with coupling holes located at the centers of both mirrors. One tunes the FP resonator to the precise resonance frequency of the source (249.9 GHz) by tuning the distance between the two mirrors. For such a multi-mode resonator, the  $Q_L = f\nu$ , where the finesse  $f = \lambda/\Delta\lambda$ , with  $\lambda$  the tuning length between successive modes, and where  $\Delta\lambda$  is the full width of a single resonator mode. [Möbius and coworkers used a FP resonator in their microwave-based ESR spectrometer at 94 GHz (91).] The superconducting magnet used provides up to 9.4 T and is sweepable, requiring a relatively low impedance. It has a homogeneity of 3 ppm over a sphere of 1-cm radius. In addition, a lower-impedance superconducting sweep coil provides more rapid sweeping over about 0.1 T.

Subsequent improvements of this transmission mode design have led to a very-high-sensitivity spectrometer where  $MN_{\min} \cong 1.5 \times 10^7$  spins/G (89, 92). Here  $M \equiv \Delta B_{\text{mod}}/\Delta B_{\text{pp}}$ , where  $\Delta B_{\text{mod}}$  is the modulation amplitude and  $\Delta B_{\text{pp}}$  is the peak-to-peak derivative line width of the broadest feature. For an  $M \approx 1/8$ , this corresponds to an  $N_{\min} \cong 1 \times 10^8$  spins/G. These sensitivity figures were

obtained from a spectrum from six oriented spin-labeled muscle fibers (radius ca  $10\ \mu\text{m}$ ) containing at most  $3 \times 10^{10}$  spins with a  $\Delta B_{\text{pp}} \approx 40\ \text{G}$  using an InSb hot electron bolometer (93) and 80-kHz field modulation. It is close to the optimum expected with the transmission design and using InSb bolometer detection (cf below) (89). Similarly low values were obtained by Lebedev (85) at 150 GHz using microwave technology. We found that in homodyne operation, hot electron bolometers perform significantly better as detectors than Schottky diode detectors (94, 95), especially when the background power can be suppressed, as in the shunt resonator discussed below, but their responses are too slow for pulse experiments.

## Signal-to-Noise Considerations

What, then, are the applications and virtues of HFHF-ESR? Clearly, the increase in absolute sensitivity demonstrated by the above results is important. Earle et al (89), in their analysis of FIR-cw-ESR spectrometers, predicted a linear increase with  $\omega$  of sensitivity, provided the technology remains unchanged. The actual situation is not so simple. Thus, as  $\omega$  and  $B_0$  increase, line widths in most (but not all) cases are observed to increase, thereby acting to reduce sensitivity. Also, as line widths increase, it becomes more difficult to provide sufficient modulation amplitude (MA), which further reduces the actual sensitivity. In addition, given the smaller wavelengths, one usually works with smaller samples, especially if they are lossy, implying that one may have to be operating closer to the  $N_{\text{min}}$ . Thus, methods to overcome the insufficient MA and/or to load up more sample into the high-frequency resonators would be of considerable value. Also, higher power levels at the FIR frequencies from stable cw sources are highly desirable (cf below).

## Applications to Molecular Dynamics in Fluids

**Improved Orientational Resolution** We now address the application of HFHF-ESR to studies of dynamics in fluids. One of the main virtues of FIR-ESR over ESR at conventional microwave frequencies is the excellent orientational resolution it provides for studies utilizing nitroxide spin labels (87, 96–98). This is clearly shown in Figure 5 (upper), which shows the positions of the resonant ESR absorptions for the canonical orientations of a typical spin probe in a powder simulation at 9.1 and at 250 GHz. At 250 GHz, the regions corresponding to molecules with their  $x$ -axis  $\parallel B_0$ ,  $y$ -axis  $\parallel B_0$ , and  $z$ -axis  $\parallel B_0$  are well separated because of the dominant role of the  $g$ -tensor. This is definitely not the case at 9.1 GHz. As a result, at 250 GHz, once motion is discernible in the spectrum, one can discern about which axis (or axes) the motion occurs. Earle et al (96) demonstrated that the 250-GHz slow-motional spectra are much more sensitive to the details of the motional dynamics than are those at 9 GHz.

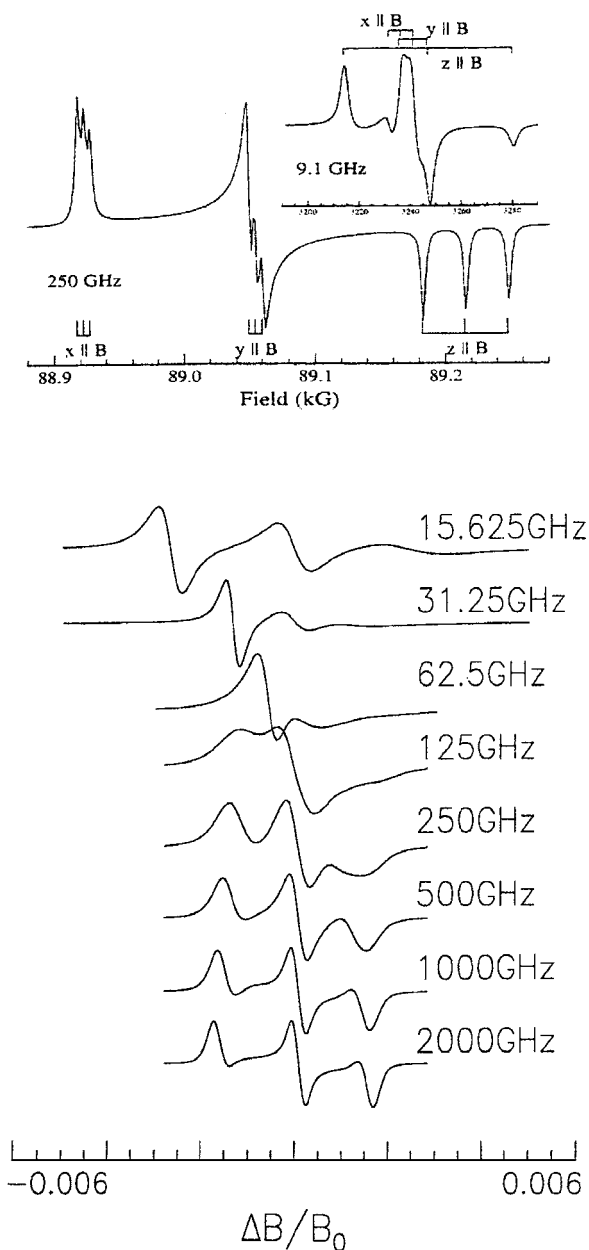


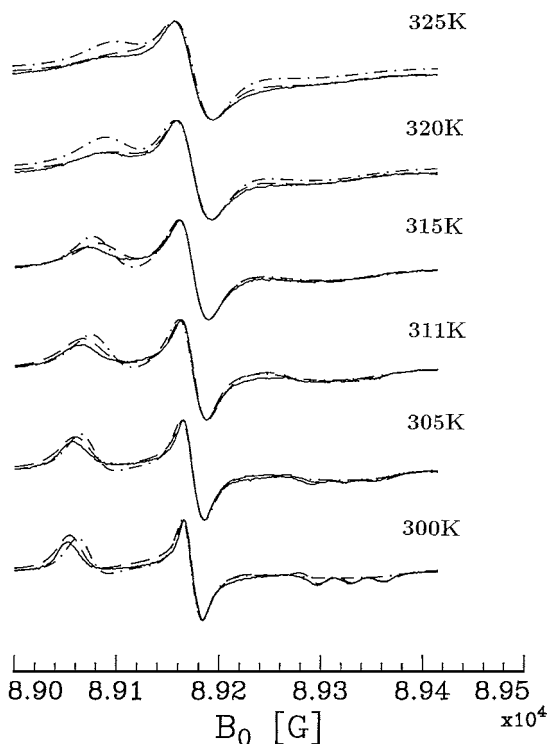
**Figure 5** (Upper) Simulation of derivative electron spin resonance spectra at 9.1 and 250 GHz for dilute powder containing a cholesterol-like nitroxide (CSL). (Short vertical lines) The fields where CSL absorbs when its  $x'$ ,  $y'$ , or  $z'$  axes are parallel to  $B_0$  (107). (Lower) Simulation of derivative electron spin resonance spectra for a nitroxide, reorienting with a rotational diffusion coefficient  $R = 10^8 \text{ s}^{-1}$  (corresponding to rotational correlation time  $\tau_R = 1.67 \text{ ns}$ ) for a wide range of frequencies.

**Model Dependence in Fast and Slow Motional Regimes** A related important feature of the 250-GHz studies is the ability to measure very accurately from (near) rigid limit spectra the magnetic tensors needed for the motional studies (87). Given these capabilities, Budil et al have shown that one can use 250-GHz ESR spectra of nitroxides in the motional narrowing regime to obtain the full anisotropic diffusion coefficient for the molecular tumbling motion (99). In fact, it was the increased sensitivity of 250-GHz ESR to the details of the motional dynamics that originally motivated the extension of the SRLS model to the slow-motional regime (44). In the earlier analyses of slow-motional ESR line shapes using the stochastic-Liouville equation, simple Markovian models were employed that just distinguish between reorientations by large, moderate, or small (i.e. Brownian) jump diffusion (96, 100). However useful these models were in fitting spectra, they beg the issue of the details of the interaction of the probe molecule with the solvent molecules. The SRLS model provides in a relatively simple manner, the essential features of a loose solvent “cage” that had been absent from the earlier models (97), but it does require increased computational efforts (44, 45).

**Dynamic Solvent Cage and Slowly Relaxing Local Structure Model** In a 250-GHz ESR study of the dynamics of several nitroxide spin probes dissolved in the glass-forming solvent ortho-terphenyl (OTP), Earle et al demonstrated how the enhanced sensitivity to rotational dynamics of the slow-motional spectra could be utilized to explore details of the dynamic solvent cage (97). They showed that the SRLS model adequately fits the model-sensitive regions of the 250-GHz spectra (cf Figure 6) and, in fact, leads to a coherent picture of the dynamics: The rotational diffusion tensors of the various probes exhibited simple behavior such that the smaller the probe the larger the diffusion coefficient. The cage relaxation rate was the slowest but was independent of the particular probe. This interesting observation appears reasonable when one considers that the cage relaxation involves just the movement of the OTP solvent molecules. In addition, the magnitude and directionality of the cage-orienting potential could be obtained. As expected, only probes comparable to or larger than the OTP molecules experienced substantial potentials, of 2–4 kT. It was possible to show that the nonlinear way in which the dynamics affects the slow-motional ESR spectra allows one to distinguish between two limiting cases. The first is that of a homogeneous liquid, but with a complex motional dynamics, (e.g. the SRLS model that was used). The second is that of an inhomogeneous liquid with a distribution of simple relaxation times (e.g. Brownian tumbling). The latter was shown to be incompatible with the 250-GHz spectra.

**High-Frequency ESR as a Faster “Snapshot” of Molecular Dynamics** Another virtue of FIR ESR is the fact that the higher the ESR frequency, the slower the motion appears to be for a given diffusion rate. This is illustrated in Figure 5 (lower), where I show simulated spectra corresponding to the same motional rate but for different ESR frequencies, ranging from 15 GHz to 2 THz. At the low frequency end,

**Figure 6** Comparison of two models for fitting effects of rotational diffusion on 250 GHz electron spin resonance spectra of spin probe of a cholesterol-like nitroxide (CSL) in ortho-terphenyl solvent. (Solid line) Experiment, (dashed line) the SRLS model, and (dashed-dotted line) simple Brownian diffusion (97).



one observes simple motionally narrowed spectra, whereas at the high frequency end, the spectra are very slow motional, almost at the rigid limit. Thus we see that the higher-frequency ESR spectra act as a faster “snapshot” of the dynamics (96, 97). This is because of the increased role of the  $g$ -tensor term, which is linear in  $B_0$  in the spin-Hamiltonian. As the orientation-dependent part of the spin-Hamiltonian  $H_1(\Omega)$  increases in magnitude with increasing  $\omega_0$  and  $B_0$ , the motional-narrowing condition  $|H_1(\Omega)|^2 \tau_R^2 \ll 1$  fails, and the spectra become slow motional.

**Multifrequency Approach to Complex Dynamics of Fluids and of Macromolecules** This snapshot feature suggests a multifrequency ESR approach to the study of the dynamics of complex fluids, such as glass-forming fluids and liquid crystals, as well as to the complex modes of motion of proteins and DNA, which should enable one to decompose the different modes according to their different timescales (45). For example, in the case of proteins, the higher frequency ESR spectra should “freeze-out” the slow overall tumbling motions, leaving only the faster internal modes of motion, whereas ESR performed at lower frequencies is sensitive to the motions on a slower timescale. In glass-forming fluids, as we

have seen, the faster motions consist of reorientations of probe molecules, whereas the slower motions relate to the dynamics of the solvent cage. Ideally then, one would want a high-sensitivity spectrometer for the study of fluids that could cover a wide range of frequencies to most effectively realize such a multifrequency approach.

The virtues of such a multifrequency approach were demonstrated in a study, using 9- and 250-GHz spectrometers, on spin-labeled mutants of the soluble protein T4 lysozyme in aqueous solution (101). In the fast timescale of the 250-GHz ESR experiment, the overall rotation was too slow to significantly affect the spectrum, so that it could satisfactorily be described by a MOMD model, which yielded good spectral resolution for the internal dynamics. Then, by fixing the internal motional parameters at the values obtained from the 250-GHz data, the SRLS fits to the 9-GHz line shapes successfully yielded the rates for the global dynamics. Thus the two types of motion were separated, and spectral resolution to these motions was significantly enhanced.

In a related 9- and 250-GHz study of segmental rotation of spin-labeled polystyrene in dilute solution, Pilar et al found systematic discrepancies between the 9- and 250-GHz results when they were separately fit by the MOMD model (102), which could again be resolved by using the SRLS model for analyzing the 9-GHz results.

In a 9-GHz study of DNA oligomers, the SRLS model was successfully utilized (103). Additional HFHF work on proteins and peptides in aqueous solution can be found in the work of Budil et al (104), Beunati et al (105), and Smirnov et al (106).

***Combining Orientational Resolution and Macroscopic Sample Alignment: Membrane Dynamics*** A striking demonstration of the excellent orientational resolution at 250 GHz in studies utilizing nitroxide spin labels was provided by a study on macroscopically aligned membranes containing a mixture of headgroups: zwitterionic PC and negatively charged phosphatidylserine (PS) using the cholesterol-like spin label CSL (107). The macroscopic alignment further enhanced the orientational resolution at 250 GHz and permitted an orientation-dependent study wherein the membrane normal could be aligned either parallel or perpendicular to the magnetic field (cf Figure 7*b*). The CSL in PC-rich membranes exhibited typical cholesterol-like behavior, such that its long axis is normal to the bilayer and its rotational diffusion rates are slow ( $R \sim 10^6 - 10^7 \text{ s}^{-1}$ ). But it exhibits markedly different behavior in PS-rich membranes, implying a strong local biaxial environment. This appears to be the first experimental evidence for local biaxiality. By contrast (107), given the poor orientational resolution at 9.1 GHz, it would not have been possible to obtain this unique motional/ordering model from the 9.1 GHz experiment. [The orientational resolution from HFHF ESR will be useful even for membrane vesicles (87, 108).]

Another application of a multifrequency approach was to determine the zero-field splitting (zfs) of high-spin Gd(III) chelates in aqueous solution using the field dependence of the dynamic frequency shift and the  $T_2$  that arise from modulation of the zfs (109).

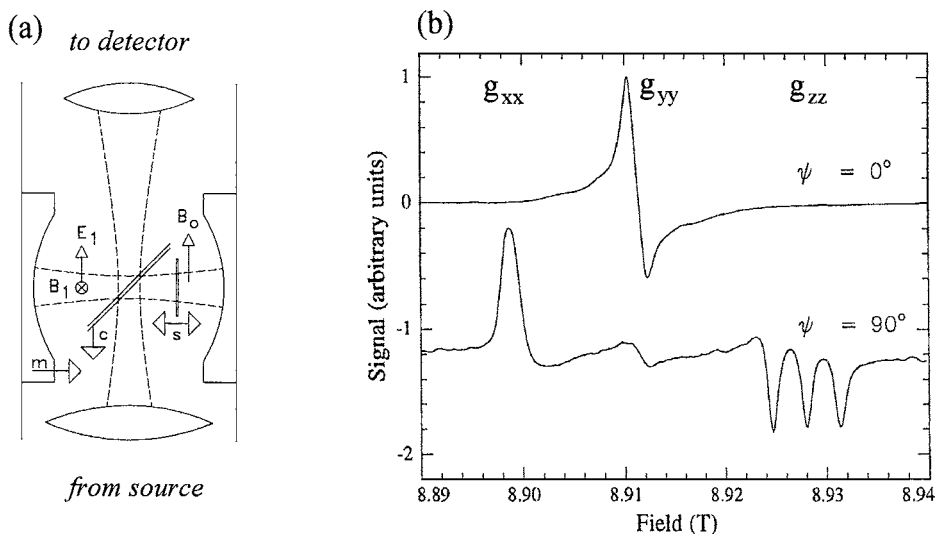


**Figure 7** (a) The relevant orientations of the millimeter-wave fields in a shunt Fabry-Perot resonator used to study an aligned sample whose normal is perpendicular to  $B_0$  (124). (b) 250-GHz derivative electron spin resonance spectra from cholesterol-like nitroxide in aligned PC-rich membrane with the membrane normal parallel ( $\Psi = 0^\circ$ ) and perpendicular ( $\Psi = 90^\circ$ ) to the magnetic field. Adjustable parts: m, mirror; s, sample, c, coupler.

## Enhancement of Spectral Resolution

HFHF ESR resolution enhancement provides the ability to resolve signals from components that differ only slightly in their  $g$ -tensors. Examples include electriles and alkalis in frozen matrices (110), resolution of thiyl radical in *Escherichia coli* (111), spin adducts for spin trapping (112), and resolution of the  $g$ -tensor of the radical pair P(700)(+)A(1)(-) in highly purified photosystem (113). These are cases where at X band the different components or species are not distinguishable, nor are their  $g$ -tensors resolvable. Additional cases where  $g$ -tensors become observable include the polyaniline family of conducting polymers (114) and various coal samples (115). Lededev's earlier work (85) had revealed the sensitivity of the nitroxide  $g$ -tensor to the "micro-environment." Earle et al (116) demonstrated that large shifts of  $g_{xx}$  occurred in frozen membrane vesicles, as the nitroxide moiety was located at different positions on the hydrocarbon chain of the lipid, with  $g_{xx}$  decreasing as the local polarity increases.

## Transition-Metal Ions

Another key application of HFHF ESR is to the study of transition-metal ions (cf Figure 8). A particularly useful special case is with ions, such as Mn(II) in its high-spin  $^5S$  state with large  $zfs$  (up to ca  $1 \text{ cm}^{-1}$ ) and small (or negligible)

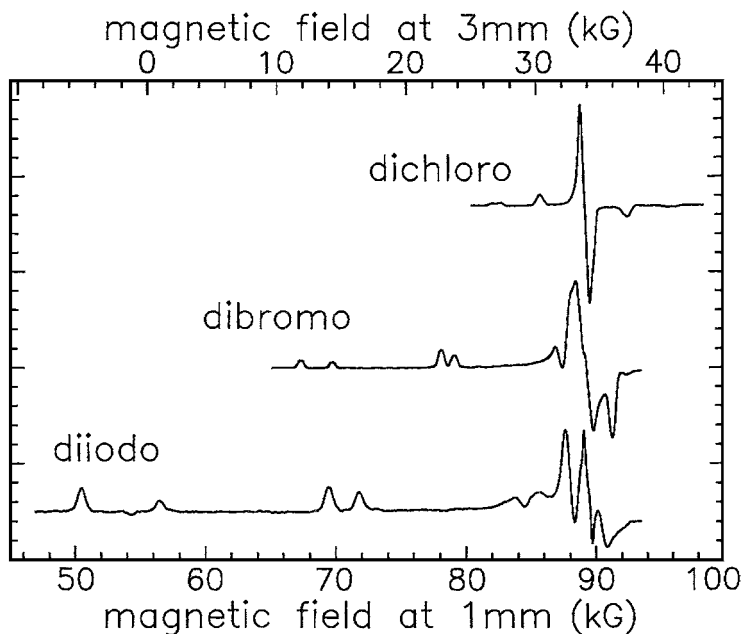


**Figure 8** Example showing that high magnetic fields and high frequencies yield simple electron spin resonance (ESR) spectra from transition metal ions with large zero-field splitting (zfs). High-field ESR spectra of Mn(II) in distorted tetrahedral environments. These are the dihalo-(triethylphosphine oxide) Mn(II) complexes. The zfs are 4.8, 15.3, and 27.3 GHz for dichloro, dibromo, and diiodo complexes, respectively. The dichloro spectrum is at 95 GHz; the other two are at 250 GHz (118).

g-tensors. In such cases the low-field ESR spectra are usually complicated because the Zeeman interaction is smaller than (or comparable to) the zfs. At high fields, the ESR spectra are simple and can be easily interpreted to extract the zfs tensor (cf Figure 8) (117, 118). In addition, non-Kramers ions, such as  $\text{Ni}^{2+}$ , pose serious problems of detection at lower frequencies, and HFHF represents an important tool for use in studying them (119–121). Such experiments typically require that one sweep the main superconducting magnet over several tesla.

In general, transition-metal ions have substantial g-tensors. Consequently, when one goes to higher fields, there will be significant g-tensor broadening in disordered solids, which will tend to obscure other features. Such problems are exacerbated by the existence of g-strain. Clearly, single-crystal studies are required to suppress this source of broadening. A single-crystal study at 250 GHz has been performed on  $\text{Ni}^{2+}$ -doped  $\text{CdCl}_6$ , where the  $\text{Ni}^{2+}$  ions are octahedrally coordinated with six  $\text{H}_2\text{O}$  molecules (92, 122). This yielded simple and easy-to-interpret spectra with two species, one showing a large (almost  $1\text{ cm}^{-1}$ ) and the other a small (about  $1/5\text{ cm}^{-1}$ ) zfs, but this is again a case of a (nearly) isotropic g-value. Some other

examples include binuclear Mn(III) Mn(IV) complexes (119), Mn(III) compounds (120), and Cr(II) (121), as well as large-spin systems [e.g. Mn<sub>12</sub>-Acetate,  $S = 10$  (122a)] and strongly exchanging systems (122b).

## Quasi-Optical Solutions to Resonators and Sample Holders for Lossy (Aqueous) Samples

In some of the above studies, certain sample characteristics provided challenges that required the development of appropriate quasi-optical solutions. Most critical is the problem of lossy samples, such as aqueous (including biological) samples and the highly conducting alkalides and electrides as well as the polyanilines. Barnes and Freed have analyzed this matter in detail for confocal FP resonators (123). They find that a flat, disk-shaped sample geometry is required to simultaneously maximize the resonator filling factor and  $Q$  by minimizing dielectric losses in the sample. The FP resonator must have provision for precisely locating the flat sample at a  $B_1$  maximum and  $E_1$  minimum near the center of the resonator, with its normal parallel to the main symmetry axis of the FP resonator. At 1.22 mm (250 GHz), the optimum thickness of an aqueous sample is only 10–25  $\mu\text{m}$ . For such small sample sizes, volumes less than 1  $\mu\text{l}$  are sufficient to fill the holder, and a high spectrometer SNR is required. Clearly, the sample holder material should have low dielectric losses and be resistant to attack by the sample. This includes very-thin (ca 0.1 mm) discs of Mylar and fused silica (123).

A more sophisticated challenge arises when oriented membranes are studied, and one wishes to tilt such lossy samples relative to the direction of the magnetic field. Barnes & Freed (124) found a special quasi-optical design for handling such samples, which they call a shunt FP resonator. In particular, they used a tilt of  $90^\circ$ , as shown in Figure 7a. The disc-shaped aqueous sample must still be kept in the  $B_1$  maximum and  $E_1$  minimum. Thus the confocal FP resonator is oriented so that its main axis is perpendicular to the incident (and exiting) beams of FIR radiation. The coupling between the (vertical) transmission beam and the (horizontal) beam mode in the FP is accomplished with an adjustable interferometer contained within the FP resonator that is tilted at  $45^\circ$  with respect to the main beam. The quasi-optical interferometer is constructed from two dielectric sheets, separated by an adjustable small gap.

## Modern Quasi-Optical Spectrometer Bridges

Given the initial successes with a quasi-optical transmission mode spectrometer, the question naturally arises as to the optimum design of a quasi-optical ESR spectrometer. I have already addressed resonator design and performance, as well as quasi-optical transmission techniques. However, microwave-based ESR spectrometers are virtually always based on bridge systems in a reflection mode. There are a number of well-known reasons for this. A principal advantage is that a reflection-mode bridge can be balanced so that the small ESR signal can be detected on a

small background. This is not generally so for the transmission mode [the shunt resonator provides a special case where it is possible (124)]. A related issue is whether the dynamic range of the detector is sufficient that the reflected carrier (i.e. non-ESR) signal does not saturate it. This problem is avoided in a well-tuned reflection-mode spectrometer in which the resonator is critically coupled. In addition, the reflection mode of operation is intrinsically more compact and more flexible in terms of the relevant quasi-optical elements.

There are at least two possible modes of operating a quasi-optical reflection bridge (89, 92). The scheme shown in Figure 9a has been implemented at Cornell (125). It is the quasi-optical analogue of a microwave bridge with a circulator, and it showed significant improvement in SNR compared with the transmission mode. It uses polarization coding techniques to separate the ESR signal from the excitation. The quarter wave plate converts horizontally polarized radiation from the source into circularly polarized radiation, which irradiates the spins. The coupling mirror and focusing mirror define the FP resonator used to enhance the  $B_1$  field at the sample. The signal emanating from the FP resonator is circularly polarized in the opposite sense. It is converted by the quarter wave plate into vertical polarization, causing it to be reflected by the polarizer, thereby directing it to the detector.

A second mode of operation shown in Figure 9b is a quasi-optical induction-mode spectrometer implemented at St. Andrew's (126). Here the horizontally polarized radiation from the source is used to irradiate the spins in the resonator. However, only the vertically polarized component of the signal passes through a polarizer, and into the detector that is operated as a homodyne mixer. One relies on the fact that in ESR, the sample's radio frequency susceptibility tensor provides a cross-polarized signal component. Earle & Freed (92) report that a polarization isolation of 30 dB for the carrier signal is a reasonable estimate.

These designs, which have actually been implemented, clearly show that there is a quasi-optical analogue to the typical designs of microwave spectrometers. The flexibility of the quasi-optics enables many variants of these basic designs. The Jones matrix formalism has proven to be a useful tool for analyzing quasi-optical designs and their relationships to equivalent microwave realizations for resonators, (89, 127). Also, quasi-optical components, such as reflecting mirrors and lenses, can readily be fabricated using standard machine shop practices. This is because the relevant wavelengths are on the order of millimeters. Given that quasi-optical components have diffraction-limited performance (90), the components will exhibit good optical performance provided that surface tolerances of the order of tenths of a millimeter are achieved.

Several groups besides the Cornell group are now operating ESR spectrometers based on such quasi-optical designs. These include the groups of Brunel (128), Budil (129), Möbius (130), and Smith (126). Good solid state sources such as phase-locked Gunn oscillators, whose outputs can be frequency multiplied, enable HFHF experiments up to almost 400 GHz (corresponding to 14-T sweepable magnets). Actually, liquid solution work has been performed using the very low dielectric loss OTP solvent up to 670 GHz with a 25-T resistive magnet and an

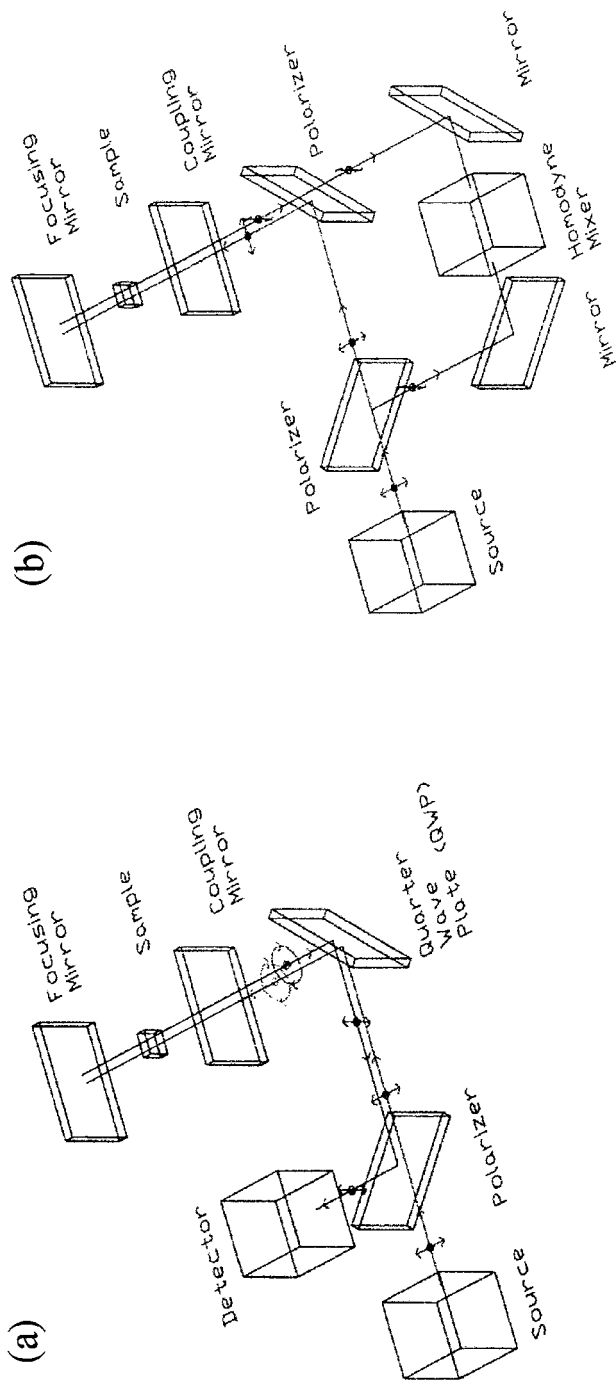


**Figure 9** Schematic diagram of (a) quasi-optical reflection bridge based on polarization coding; (b) quasi-optical induction-mode reflection bridge (92).

FIR laser (131). FIR lasers are an appropriate solution for work above 400 GHz, but they are not nearly as convenient to operate as the stable solid state sources. Also, large resistive magnets require major dedicated facilities.

## Other Instrumental Features

**Limitations of Magnetic-Field Modulation** As discussed above, a limiting SNR feature of quasi-optical spectrometers is the available modulation amplitude. In many cases,  $\Delta B_{\text{mod}} \ll \Delta B_{\text{pp}}$  (i.e.  $M \ll 1$ ). It is probably not practical to use  $\Delta B_{\text{mod}} > 20\text{--}25$  G because of sample heating effects. Multi-quantum (photon) ESR as defined and developed by Hyde and coworkers might be a useful technique to replace  $\Delta B_{\text{mod}}$  (73).

**Current Pulse Techniques** Another approach is to employ pulse techniques because they remove the need for field modulation. Most HFHF pulse spectrometers to date are limited by the weak coherent radiation sources available for the pulsing (132–136). Typically pulses are of ca 20- to 100-mW intensities, which correspond to  $\pi/2$  pulses of ca 50–100 ns using small single-mode resonators at 95–150 GHz. This has proved satisfactory for work at very low temperatures, where relaxation times are very long (137). However, given the focus of this review on techniques for fluids at or near room temperature, these spectrometers are not satisfactory for such purposes. For example, at 250 GHz, one can have nitroxide  $T_2$ s as short as a few nanoseconds. It would be impossible to rotate such electron spins by a  $\pi/2$  pulse lasting 50–100 ns. In addition, such long pulses will have very small spectral bandwidths (e.g. about 10 MHz for a 60-ns  $\pi/2$  pulse), so only a small fraction of the spins would be irradiated. The question then is how to achieve higher-power, preferably coherent, pulses. Weis et al have used a gyrotron at 140 GHz to provide a “pump” power of ca 100 W in dynamic nuclear polarization experiments (138). For ESR detection, one can use the gyrotron to provide short pulses for FIDs (138). But because the gyrotron signal is not clean, it might be better to use a standard, stable low-power cw source for detection of, for example, the spin-inversion recovery after a gyrotron pulse (139). There has been some success with the use of FIR lasers at 604 GHz, which produced 100-ns pulses (140). Here quasi-optical techniques of beam splitting followed by time delay of one of them can lead to a two (phase coherent) pulse spin echo sequence, but it becomes difficult to step out the pulse separation. Instead, two separate lasers can be used, but one must adjust them to exact resonance, a difficult task (140). In general, phase coherences between such pulses remains a concern.

**Development of Intense Coherent Pulse Source for 95 GHz** It would seem that the best approach is to use the weak coherent pulses that can be generated with existing solid state sources, and then to amplify them by analogy to pulsed microwave spectrometers. At present, at Cornell we have succeeded in developing a 1-kW pulse source at 95 GHz, with pulse widths as small as 2.5–5 ns (141).

A phase-locked Gunn oscillator and PIN diode switches provide the 50-mW pulses (with a nominal minimum pulse spacing of 10 ns). They are amplified by an extended interaction klystron amplifier (EIK/A). This system has full quadrature phase-cycling capability. These are the properties required to perform pulse and possibly 2D-FT-ESR experiments of the sort described earlier in this chapter for the 9- to 17-GHz microwave regime. This high-power pulse source is used with a quasi-optical bridge configured as an induction-mode reflection bridge spectrometer to minimize the magnitude of any reflected pulses reaching the detector (141). It also operates in a heterodyne fashion with a 0.7-GHz intermediate frequency. This is needed because Schottky diode detectors, which have response times fast enough to permit nanosecond data acquisition rates, have poor  $1/f$  noise performance at lower frequencies, especially below 1 MHz.

The EIK/A approach could be extended to 220–250 GHz (142). Another possibility for a millimeter-pulse amplifier could be the gyrokylystron (LC Brunel, private communication), which is currently being developed (143, 144). Also orotrons [which are free electron masers based on the Smith-Purcell effect (145)] are under consideration for such purposes (K Möbius, private communication).

The advent of high-power, pulsed spin-echo and 2D-ESR at HFHF should combine the excellent orientational resolution and “fast-snapshot times” of this frequency range, with the ability to look directly at the spin relaxation processes, e.g. to be able to distinguish homogeneous ( $T_2^{-1}$ ) line widths from inhomogeneous line broadening, which proved useful for studies of complex fluids at microwave frequencies.

## ESR IMAGING

### Dynamic Imaging of Diffusion

Like NMR imaging (or magnetic resonance imaging), ESR poses instrumental challenges, but it has a number of interesting applications. A review of the ESR imaging field was provided in 1991 (146) and more recently by Eaton et al (147). Here, with limited space remaining, I continue to briefly review applications to studies of molecular dynamics in fluids. The Freed group has developed a powerful method for measuring macroscopic translational diffusion over the range of  $D$  from  $10^{-5}$  to  $10^{-10}$  cm<sup>2</sup>/s, which they call dynamic-imaging of diffusion (DID)-ESR (148). This is based on the use of cw-ESR imaging in the presence of a static magnetic field gradient. One obtains ESR spectra as a function of time, starting with an inhomogeneous distribution of spins. The FT of the spectra vs time are readily fit to the Fick’s law diffusion equation to provide the diffusion coefficient typically to  $\pm 10\%$  accuracy. Extensive studies using this method, especially for diffusion in oriented phospholipid membranes, have been reviewed previously (149). In a study of diffusion of different size nitroxide probes in a smectic liquid crystal by DID-ESR, it was possible to distinguish the anisotropy in the diffusion

coefficient corresponding to diffusion parallel to the direction of alignment ( $D_{\parallel}$ ) and perpendicular to that direction ( $D_{\perp}$ ) (150). These results could successfully be rationalized in terms of a free-volume theory, adapted for liquid crystals.

In a variant of this approach, viz by spectral-spatial imaging, the spatial direction vs time provided the macroscopic  $D_{\text{macro}}$ , whereas the concentration dependence of the imaged spectrum arising from the initial inhomogeneous spin distribution provided the  $D_{\text{micro}}$  from Heisenberg spin exchange (151). It was found, in an oriented lipid membrane, that  $D_{\text{micro}} > D_{\text{macro}}$  by about a factor of 4.

More recently, DID-ESR was applied to the study of a polydisperse polymer (i.e. with a wide distribution of molecular weights) (152). A careful analysis allowed the determination of the molecular weight dependence of the diffusion coefficients to compare with existing theories. Schlick and coworkers have used spectral-spatial imaging to determine  $D$  for monodisperse probes in polymer solutions (153–155). High-field ESR imaging (156) has yet to be applied to fluids.

## FT-ESR Imaging

The extension of ESR imaging to the FT domain, as in NMR, required special techniques for generating pulsed field gradients. Using a specially designed low-impedance field-gradient coil of small dimensions, and a fast MOSFET driver, it was possible to achieve gradient pulses of 100 G/cm lasting for ca 90–100 ns. This technology permitted FT spatial imaging by the phase-encoded method (157). It even led to a successful spatially resolved 2D-ELDOR experiment, wherein the exchange cross peaks due to HE arising from  $^{14}\text{N}$  vs  $^{15}\text{N}$  nitroxides, which were spatially separated in a phantom, could be resolved (158). This technology is worthy of further development to shorter (less than 40–50 ns rise and fall times) and possibly more intense gradients (e.g. 200 G/cm). This would permit an FT version of DID-ESR, which will more directly (148), and perhaps more accurately, lead to measurements of  $D$  than the cw method. It would also open the possibility of using short-pulsed field gradients to suppress unwanted coherence pathways when using complex pulse sequences (e.g. for DQC studies, cf above). This is an approach commonly used in NMR (159), where it is much less demanding.

## Low-Frequency ESR Imaging: Biomedical Applications

The development of ESR imaging for biomedical applications has posed a number of significant challenges (160). The problem of microwave dielectric losses at higher frequencies has restricted these developments to  $\leq 1$  GHz, with the regime of 250–500 MHz being favored (as in NMR) (160–162). However, this regime corresponds to reduced SNR because of the lower frequencies used, and substantially longer dead times,  $\tau_d$  in pulse spectrometers (163). The  $\tau_d$  nominally are inversely proportional to  $\omega^{-1}$  (cf above). Nevertheless, the greater sensitivity per spin compared with NMR, and the ability to spin label, and/or to use spin probes, makes it suitable for such studies as drug delivery and oxygen perfusion. (160).

## SUMMARY

The challenges for ESR as described above continue to be (a) the demands of fast nanosecond time resolution, especially the need to minimize spectrometer dead times in pulsed ESR, (b) the development of very intense and short radiation pulses to benefit from full irradiation schemes for this “magnetic-dipole-allowed” spectroscopy, (c) new and improved quasi-optical methods to enhance high-frequency ESR; (d) the development of high-power, coherent pulse sources for high-frequency ESR, and (e) the development of rapid pulsed-field gradients for time-domain ESR imaging and for suppression of unwanted coherence pathways in multiple coherence and other multi-pulse ESR methods.

This review has emphasized how recent developments in these technologies have led to powerful methods for the study of molecular dynamics in a range of complex fluids, as well as in the capability of measuring large molecular distances. It is expected that further developments will greatly improve ESR capabilities for such studies (and this will necessarily provide more sophisticated computational challenges), as well as for a range of other applications either only hinted at or omitted for lack of space in this review.

## ACKNOWLEDGMENTS

I wish to especially thank Drs. Peter P Borbat and Keith A Earle for their critical reading and their many suggestions that improved this chapter, as well as Professor Jozef K Moscicki for helpful comments and assistance. This work was supported by grants from the NSF and NIH.

Visit the Annual Reviews home page at [www.AnnualReviews.org](http://www.AnnualReviews.org)

## LITERATURE CITED

- Ernst RR, Bodenhausen G, Wokaun A. 1987. *Principles of Nuclear Magnetic Resonance in One and Two Dimensions*. Oxford, UK: Clarendon
- Dalton LR, Bain A, Young CL. 1990. *Annu. Rev. Phys. Chem.* 41:389–407
- Stehlik D, Möbius K. 1997. *Annu. Rev. Phys. Chem.* 48:739–78
- Levanon H, Möbius K. 1997. *Annu. Rev. Biophys. Biomol. Struct.* 26:495–540
- Mims WB, Nassau K, McGee JD. 1961. *Phys. Rev.* 123:2059
- Mims WB, Peisach J. 1989. See Ref. 16, pp. 1–57
- Salikhov KM, Tsvetkov YD. 1979. In *Time-domain Electron Spin Resonance*, ed. L Kevan, RN Schwartz, pp. 231–77. New York: Wiley
- Salikhov KM, Semyenov AG, Tsvetkov YD. 1976. *Electron Spin Echoes and Their Applications*. Novosibirsk, Russia: Nauka
- Schweiger A. 1993. *Appl. Magn. Reson.* 5:229–64
- Willer M, Granwehr J, Forrer J, Schweiger A. 1998. *J. Magn. Reson.* 133:46–52
- Jeschke G, Schweiger A. 1996. *Mol. Phys.* 88:355–83
- Thomann H, Bernardo M. 1990. *Chem. Phys. Lett.* 169:5–11

13. Hoffman BM, Davoust CE, Doan PE. 1996. *J. Magn. Reson. A* 119:38–44
14. Kevan L, Schwartz RN, eds. 1979. *Time Domain Electron Spin Resonance*. New York: Wiley Intersci.
15. Kevan L, Bowman MK, eds. 1990. *Modern Pulsed and Continuous Wave ESR*. New York: Wiley
16. Hoff A, ed. 1989. *Advanced EPR: Applications in Biology Biochemistry*. Amsterdam: Elsevier
17. Hornak JP, Freed JH. 1986. *J. Magn. Reson.* 67:501–18
18. Eliav U, Freed JH. 1984. *J. Chem. Phys.* 88:1277–80
19. Panferov YF, Grinberg OY, Dubinskii AA, Lebedev YS. 1984. *Dokl. Phys. Chem.* 278:888–90
20. Millhauser GL, Freed JH. 1984. *J. Chem. Phys.* 81:37–48
- 20a. Gorcester J, Millhauser GL, Freed JH. 1989. See Ref. 16, Ch. 5
21. Gorcester J, Freed JH. 1986. *J. Chem. Phys.* 85:5375–77
22. Millhauser GL, Gorcester J, Freed JH. 1987. In *Electron Magnetic Resonance of the Solid State*, ed. JA Weil, pp. 571–98. Ottawa, Ont.: Can. Chem. Soc.
23. Dobbert O, Prisner T, Dinse KP. 1986. *J. Magn. Reson.* 70:173–75
24. Angerhofer A, Toporowicz M, Bowman M, Norris JR, Levanon H. 1988. *J. Phys. Chem.* 92:7164–66
25. Bowman MK. 1990. See Ref. 165, pp. 1–42
26. Gorcester J, Freed JH. 1988. *J. Chem. Phys.* 88:4678–93
27. Angerhofer A, Massoth RJ, Bowman MK, Israel J. 1988. *Chemistry* 28:227–38
28. Gorcester J, Rananavare SB, Freed JH. 1989. *J. Chem. Phys.* 90:5764–86
- 28a. Miiick SM, Millhauser GL. 1994. *J. Magn. Reson. B* 104:81–84
29. Patyal BR, Crepeau RH, Gamliel D, Freed JH. 1990. *Chem. Phys. Lett.* 175: 445–52
30. Patyal BR, Crepeau RH, Gamliel D, Freed JH. 1990. *Chem. Phys. Lett.* 175:453–506
31. Froncisz W, Hyde JS. 1982. *J. Magn. Reson.* 47:515
32. Hornak JP, Freed JH. 1985. *J. Magn. Reson.* 62:311–13
33. Pfenninger S, Forrer J, Schweiger A. 1988. *Rev. Sci. Instrum.* 59:752
34. Patyal BR, Lee S, Saxena SK, Crepeau RH, Freed JH. 1994. *Chem. Phys. Lett.* 221:397–406
35. Crepeau RH, Saxena SK, Lee S, Patyal BR, Freed JH. 1994. *Biophys. J.* 66:1489–504
36. Sastry VSS, Polimeno A, Crepeau RH, Freed JH. 1996. *J. Chem. Phys.* 105:5753–72
37. Sastry VSS, Polimeno A, Crepeau RH, Freed JH. 1996. *J. Chem. Phys.* 105:5773–91
38. Xu D, Crepeau RH, Ober CK, Freed JH. 1996. *J. Phys. Chem.* 100:15873–85
39. Lee S, Budil D, Freed JH. 1994. *J. Chem. Phys.* 101:5529–58
- 39a. Saxena SK, Freed JH. 1997. *J. Phys. Chem. A* 101:7998–8008
40. Ge M, Field KA, Aneja R, Holowka D, Baird B, Freed JH. 1999. *Biophys. J.* 77:925–33
41. Meirovitch E, Nayeem A, Freed JH. 1984. *J. Phys. Chem.* 88:3454–65
42. Polnaszek CF, Freed JH. 1975. *J. Phys. Chem.* 79:2283–306
43. Freed JH. 1977. *J. Chem. Phys.* 66:4183–99
44. Polimeno A, Freed JH. 1995. *J. Phys. Chem.* 99:10995–1006
45. Liang ZC, Freed JH. 1999. *J. Phys. Chem. B* 103:6384–96
- 45a. Dubinskii AA, Maresch GG, Spiess HW. 1994. *J. Chem. Phys.* 100:2437
46. Borbat PP, Crepeau RH, Freed JH. 1997. *J. Magn. Reson.* 127:155–67
47. Rinard GA, Quine RW, Harbridge JR, Song R, Eaton GR, et al. 1999. *J. Magn. Reson.* 140:218–27

48. Piarecki W, Froncisz W, Hyde JS. 1996. *Rev. Sci. Instrum.* 67:1896–904
49. Davis JL, Mims WB. 1981. *Rev. Sci. Instrum.* 52:131–32
50. Dulcic A, Crepeau RH, Saarinen TR, Freed JH. 1989. *J. Magn. Reson.* 84:184–90
51. Farkas ZD. 1986. *IEEE Transact. Microwave Theory Tech.* 34:1036–43
52. Gorcester J, Freed JH. 1988. *J. Magn. Reson.* 78:292–301
53. Gorcester J, Millhauser GL, Freed JH. 1990. In *Advances in Pulsed and Continuous Wave Electron Spin Resonance*, ed. L Kevan, M Bowman, 3:119–94. New York: Wiley
54. Saxena S, Freed JH. 1997. *J. Magn. Reson.* 124:439–54
55. Patyal B, Crepeau RH, Freed JH. 1997. *Biophys. J.* 73:2201–20
56. Borbat P, Crepeau RH, Ge M, Freed JH. 1999. *22nd Int. EPR Symposium, Denver, CO*, August
57. Piluschau M, Dinse KP. 1994. *J. Magn. Reson. A* 109:181–91
58. Piluschau M, Schweitzer P, Dinse K-P, Fuchs D, Rietschel H, et al. 1995. *Chem. Phys. Lett.* 24:615–21
59. Kababya S, Luz Z, Goldfarb D. 1994. *J. Am. Chem. Soc.* 116:5805–13
60. Kababya S, Bilkis I, Goldfarb D. 1996. *J. Am. Chem. Soc.* 118:9680–90
61. McLauchlan KA. 1990. See Ref. 15, pp. 285–363
62. Eveson RW, McLauchlan KA. 1999. *Mol. Phys.* 96:133–42
63. Forbes MDE. 1993. *Rev. Sci. Instrum.* 64:397–402
64. Forbes MDE. 1992. *J. Phys. Chem.* 96:7836–39
65. Yin J, Feix JB, Hyde JS. 1990. *Biophys. J.* 58:713–20
66. Subczynski WK, Lewis RNAH, McElhaney RN, Hodges RS, Hyde JS, et al. 1998. *Biochemistry* 37:3156
67. Haas DA, Sugano T, Mailer C, Robinson BH. 1993. *J. Phys. Chem.* 97:2914–21
68. Eaton GR, Eaton SS, Berliner LJ, eds. 2000. *Distance Measurements in Biological Systems by EPR*. New York: Kluwer
69. Saxena S, Freed JH. 1996. *Chem. Phys. Lett.* 251:102–10
70. Saxena S, Freed JH. 1997. *J. Chem. Phys.* 107:1317–40
71. Borbat PP, Freed JH. 1999. *Chem. Phys. Lett.* 313:145–54
72. Borbat PP, Freed JH. 2000. *Biol. Magn. Reson.* 19:Ch. 9
73. Strangeway RA, Mchaourab HS, Luglio JR, Francisz W, Hyde JS. 1995. *Rev. Sci. Instrum.* 66:4516–28
74. Raitsimring AM, Salikhov KM. 1985. *Bull. Magn. Reson.* 7:184–217
75. Milov AD, Salikhov KM, Shirov MD. 1981. *Sov. Phys. Solid State* 23:565–69
76. Milov AD, Maryasov AG, Tsvetkov YD. 1998. *Appl. Magn. Reson.* 15:107–43
77. Kurshev VV, Raitsimring AM, Tsvetkov YD. 1989. *J. Magn. Reson.* 81:441–54
78. Raitsimring AM, Crepeau RH, Freed JH. 1995. *J. Chem. Phys.* 102:8746–62
79. Abragam A. 1961. *The Principles of Nuclear Magnetism*. New York: Oxford Univ. Press
80. Pfannebecker V, Klos H, Hubrich M, Volkmer T, Heuer A, et al. 1996. *J. Phys. Chem.* 100:13428
81. Feher G, Richards PL. 1967. In *Magnetic Resonance in Biological Systems*, ed. A Ehrenberg, BG Malmström, T Vänngård, pp. 141–44. New York: Pergamon
82. Brakett GC, Richards PL. 1971. *J. Chem. Phys.* 54:4383–401
83. Champion PM, Sievers AL. 1980. *J. Chem. Phys.* 72:1569–82
84. Grinberg OY, Dubinskii AA, Shuvalov VF, Oranskii LA, Kurochkin VA, et al. 1976. *Dokl. Phys. Chem.* 230:923
85. Lebedev YS. 1990. See Ref. 65, pp. 365–404
86. Lynch B, Earle K, Freed JH. 1988. *Rev. Sci. Instrum.* 59:1345–51
87. Budil DE, Earle KA, Lynch WB, Freed JH. 1989. In *Advanced EPR Applications in*

- Biology and Biochemistry*, ed. A Hoff, 8:307–40. Amsterdam: Elsevier
88. Barra AL, Brunel LC, Robert JB. 1990. *Chem. Phys. Lett.* 165:107–9
89. Earle KA, Budil DE, Freed JH. 1996. *Adv. Magn. Opt. Reson.* 19:253–323
90. Goldsmith PS. 1998. *Quasioptical Systems: Gaussian Beam Quasioptical Propagation and Applications*. New York: IEEE Press
91. Haindl E, Möbius K, Oloff H. 1985. *Z. Naturforsch. Teil A* 40:169–72
92. Earle KA, Freed JH. 1999. *Appl. Magn. Reson.* 16:247–72
93. Tannenwald PE. 1980. *Int. J. Infrared Millimeter Waves* 1:159–73
94. Lucas C, Amingual C, Chataud JP. 1994. *J. Phys. Colloq.* 4:177–82
95. Nilges MJ, Smirnov AI, Clarkson RB, Belford RL. 1999. *Appl. Magn. Reson.* 16:167–83
96. Earle KA, Budil DE, Freed JH. 1993. *J. Phys. Chem.* 97:13289–97
97. Earle KA, Moscicki J, Polimeno A, Freed JH. 1997. *J. Chem. Phys.* 106:9996–10015
98. Earle KA, Moscicki J, Polimeno A, Freed JH. 1998. *J. Chem. Phys.* 109:10525–26
99. Budil DE, Earle KA, Freed JH. 1993. *J. Phys. Chem.* 97:1294–303
100. Budil DE, Lee S, Saxena S, Freed JH. 1996. *J. Magn. Reson. A* 120:155–89
101. Barnes J, Liang Z, Mchaourab H, Freed JH, Hubbell WL. 1999. *Biophys. J.* 76:3298–306
102. Pilar J, Labsky J, Marek A, Budil DE, Earle KA, et al. 2000. *Macromolecules.* 33:4438–44
103. Liang Z, Bobst AM, Keyes RS, Freed JH. 2000. *J. Phys. Chem. B.* 104:5372–81
104. Budil DE, Kolaszkowski SV, Perry A, Valaprasad C, Johnson F, et al. 2000. *Biophys. J.* 78:430–38
105. Beunati M, Gerfen GJ, Martinez GV, Griffin RG, Singel DJ, Millhauser GL. 1999. *J. Magn. Reson.* 139:281–86
106. Smirnov AI, Belford RL, Clarkson RB. 1998. *Biol. Magn. Reson.* 14:83–108
107. Barnes JP, Freed JH. 1998. *Biophys. J.* 75:2532–46
108. Marsh D, Gaffney B. 1998. *Proc. Natl. Acad. Sci. USA* 95:12940–43
109. Clarkson RB, Smirnov AI, Smirnova TI, Kang H, Belford RL, et al. 1998. *Mol. Phys.* 95:1325–32
110. Shin DH, Dye JL, Budil DE, Earle KA, Freed JH. 1993. *J. Phys. Chem.* 97:1213–19
111. Vanderdonk WA, Stubbe J, Gerfen GJ, Bellow BF, Griffin RG. 1995. *J. Am. Chem. Soc.* 117:8908–16
112. Smirnova TI, Smirnov AI, Clarkson RB, Belford RL, Kotake Y, et al. 1997. *J. Phys. Chem. B* 101:3877–85
113. vanderEst A, Prisner T, Bittl R, Fromme P, Lubitz W, et al. 1997. *J. Phys. Chem. B* 101:1437–43
114. Tipikin DS, Earle KA, Freed JH. 1999. *Polym. Sci. Ser. B* 41:1043–47
115. Clarkson RB, Wang W, Brown DR, Crookham HC, Belford RL. 1990. *Fuel* 69:1405–11
116. Earle KA, Moscicki JK, Ge M, Freed JH. 1994. *Biophys. J.* 66:1213–21
117. Lynch WB, Boorse RS, Freed JH. 1993. *J. Am. Chem. Soc.* 115:10909–15
118. Wood RM, Stucker DM, Jones LM, Lynch WB, Misra SK, Freed JH. 1999. *Inorg. Chem.* 38:5384–88
119. Policar C, Kruepling M, Frapart Y-M, Un S. 1998. *J. Phys. Chem. B* 102 10391–98
120. Barra A-L, Gatteschi D, Sessoli R, Abbati GL, Cornia A, et al. 1997. *Angew. Chem.* 36:2329–31
121. Telsler J, Pardi LA, Krzystek J, Brunel LC. 1998. *Inorg. Chem.* 37:5769–75
122. Misra S, Earle KA, Freed JH. 1999. 22nd *Int. EPR Symp., Denver, CO*, August
- 122a. Cage B, Cevc P, Blinc R, Brunel LC, Dalal NX. 1998. *J. Magn. Reson.* 135:178–84
- 122b. Hill S, Perenboom JAAJ, Dalal NS,

- Hathaway T, Stalcup T, et al. 1998. *Phys. Rev. Lett.* 80:2453–56
123. Barnes JP, Freed JH. 1997. *Rev. Sci. Instrum.* 68:2838–46
124. Barnes JP, Freed JH. 1998. *Rev. Sci. Instrum.* 69:3022–27
125. Earle KA, Tipikin DS, Freed JH. 1996. *Rev. Sci. Instrum.* 67:2502–13
126. Smith GM, Le Surf JCG, Mitchell RH, Riedi PC. 1998. *Rev. Sci. Instrum.* 69:3924–27
127. Budil DE, Ding Z, Smith GR, Earle KA. 2000. *J. Magn. Reson.* 144:20–34
128. Hassan AK, Maniero A-L, van Tol H, Saylor C, Brunel LC. 1999. *Appl. Magn. Reson.* 16:299–308
129. Cardin JT, Kolaczowski SV, Anderson JR, Budil DE. 1999. *Appl. Magn. Reson.* 16:273–92
130. Fuchs MR, Prisner TF, Möbius K. 1999. *Rev. Sci. Instrum.* 70:3681–83
131. Hassan A, van Tol H, Maniero AL, Brunel LC, Earle KA, Freed JH. 1999. In *Physical Phenomena at High Magnetic Fields-III*, ed. Z Fisk, L Gurkov, JR Schrieffer, pp. 453–56. Singapore: World Sci.
132. Prisner TF. 1997. *Adv. Magn. Opt. Reson.* 20:245–300
133. Allgeier J, Disselhorst JAJM, Weber RT, Wenckebach WTh, Schmidt J. 1990. See Ref. 165, pp. 267–84
134. Bresignunov AY, Dubinskii AA, Krimov VN, Petrov YG, Poluektov OG, Lebedev YS. 1991. *Appl. Magn. Reson.* 2:715
135. Bennati M, Farrar CT, Bryant JA, Inati SJ, Weis V, et al. 1999. *J. Magn. Reson.* 138:232–43
136. Rohrer M, Gast P, Möbius K, Prisner TF. 1996. *Chem. Phys. Lett.* 259:523–30
137. Gromov I, Krymov V, Manikandan P, Arieli D, Goldfarb D. 1999. *J. Magn. Reson.* 139:8–17
138. Weis V, Bennati M, Rosay M, Bryant JA, Griffin RG. 1999. *J. Magn. Reson.* 140:293–99
139. Calame JP, Danly BG, Garven M. 1999. *Phys. Plasmas* 6:2614–25
140. Moll HP, Kutter C, van Tol J, Zuckerman H, Wyder P. 1999. *J. Magn. Reson.* 137:46–58
141. Earle KA, Dunnam C, Borbat PP, Freed JH. 2000. *Am. Phys. Soc. Abstr.* 45:542
142. Mead J, McIntosh R. 1991. *Natl. Telesyst. Conf. Proc.* 1:343–46
143. Blank M, Danly BG. 1999. *Phys. Plasmas* 6:4405–9
144. Dumesh BS, Surin LA. 1996. *Rev. Sci. Instrum.* 67:3458–64
145. Risaliti R, Ronchi L, Scordino A. 1988. *Infrared Phys.* 28:353–61
146. Eaton GR, Eaton SS, Ohno K, eds. 1991. *EPR Imaging and in Vivo EPR*. Boca Raton, FL: CRC Press. 321 pp.
147. Eaton GR, Eaton SS, Rinaud GA. 1998. In *Spatially Resolved Magnetic Resonance*, ed. P Blümer, P Blümich, R Botto, E Fukushima. New York: Weinheim
148. Moscicki JK, Shin YK, Freed JH. 1991. See Ref. 146, pp. 189–219
149. Freed JH. 1994. *Annu. Rev. Biophys. Biomol. Struct.* 23:1–25
150. Moscicki JK, Shin YK, Freed JH. 1993. *J. Chem. Phys.* 99:634–49
151. Shin YK, Ewert U, Budil DE, Freed JH. 1991. *Biophys. J.* 59:950–57
152. Xu D, Hall E, Ober CK, Moscicki JK, Freed JH. 1996. *J. Phys. Chem.* 100:15856–66
153. Schlick S, Pilar J, Kweon SC, Vacik J, Gao Z, Labsky J. 1995. *Macromolecules* 28:5780–88
154. Gao Z, Pilar J, Schlick S. 1996. *J. Phys. Chem.* 100:8430–35
155. Degtyarov YN, Schlick S. 1999. *Langmuir* 15:5040–47
156. Smirnov AI, Poluektov OG, Lebedev YA. 1992. *J. Magn. Reson.* 97:1–12
157. Ewert U, Crepeau RH, Dunnam CR, Xu D, Lee S, Freed JH. 1991. *Chem. Phys. Lett.* 184:25–33
158. Ewert U, Crepeau RH, Lee S, Dunnam CR, Xu D, Freed JH. 1991. *Chem. Phys. Lett.* 184:34–40

- 
159. Bax A, De Jong PG, Mehlkopf AF, Smidt J. 1980. *Chem. Phys. Lett.* 69:567-72
160. Berliner LJ, ed. 2000. *Biological Magnetic Resonance*. Vol. 18. *In Vivo EPR: Theory and Applications*. New York: Kluwer Acad./Plenum. Ch. 4
161. Koscielniak J. 2000. See Ref. 160. In press
162. Kuppusamy P, Chzhan M. 2000. See Ref. 160. Ch. 6
163. Subramanian S, Mitchell JB, Murali MC. 2000. See Ref. 160. Ch. 7



## CONTENTS

Fifty Years in Physical Chemistry: Homage to Mentors, Methods, and Molecules, <i>Dudley Herschbach</i>	1
SURFACE PLASMON RESONANCE IMAGING MEASUREMENTS OF ULTRATHIN ORGANIC FILMS, <i>Jennifer M. Brockman, Bryce P. Nelson, Robert M. Corn</i>	41
Delayed Ionization and Fragmentation En Route to Thermionic Emission: Statistics and Dynamics, <i>E. E. B. Campbell, R. D. Levine</i>	65
Spatially Heterogeneous Dynamics in Supercooled Liquids, <i>M. D. Ediger</i>	99
Generalized Born Models of Macromolecular Solvation Effects, <i>Donald Bashford, David A. Case</i>	129
Chemical Dynamics at Metal Surfaces, <i>John C. Tully</i>	153
Peptides and Proteins in the Vapor Phase, <i>Martin F. Jarrold</i>	179
Effective Interactions Between Electric Double Layers, <i>Jean-Pierre Hansen, Hartmut Löwen</i>	209
Transient Laser Frequency Modulation Spectroscopy, <i>Jean-Pierre Hansen, Hartmut Löwen</i>	243
Motion and Disorder in Crystal Structure Analysis: Measuring and Distinguishing Them, <i>H. B. Bürgi</i>	275
Quantitative Atom-Atom Potentials from Rotational Tunneling: Their Extraction and Their Use, <i>M. R. Johnson, G. J. Kearley</i>	297
Decoding the Dynamical Information Embedded in Highly Mixed Quantum States, <i>John C. Keske, Brooks H. Pate</i>	323
Large-Scale Shape Changes in Proteins and Macromolecular Complexes, <i>Michael E. Wall, Stephen C. Gallagher, Jill Trehwella</i>	355
Reflection Absorption Infrared Spectroscopy and the Structure of Molecular Adsorbates on Metal Surfaces, <i>Michael Trenary</i>	381
The Dynamics of Noble Gas-Halogen Molecules and Clusters, <i>Andreas Rohrbacher, Nadine Halberstadt, Kenneth C. Janda</i>	405
Molecular Dynamics Simulation of Nucleic Acids, <i>Thomas E. Cheatham III, Peter A. Kollman</i>	435
Chemistry and Microphysics of Polar Stratospheric Clouds and Cirrus Clouds, <i>Mark A. Zondlo, Paula K. Hudson, Anthony J. Prenni, Margaret A. Tolbert</i>	473
Monte Carlo Methods in Electronic Structures for Large Systems, <i>Arne Lüchow, James B. Anderson</i>	501
Thermodynamics of the Size and Shape of Nanocrystals: Epitaxial Ge on Si(001), <i>R. Stanley Williams, Gilberto Medeiros-Ribeiro, Theodore I. Kamins, Douglas A. A. Ohlberg</i>	527
Semiclassical Calculation of Chemical Reaction Dynamics via Wavepacket Correlation Functions, <i>David J. Tannor, Sophya Garashchuk</i>	553
Self-Assembled Ceramics Produced by Complex-Fluid Templatation, <i>Daniel M. Dabbs, Ilhan A. Aksay</i>	601
Theoretical Studies of Atomic-Scale Processes Relevant to Crystal Growth, <i>Hannes Jónsson</i>	623
New Technologies in Electron Spin Resonance, <i>Jack H. Freed</i>	655
Multidimensional Femtosecond Correlation Spectroscopies of Electronic and Vibrational Excitations, <i>Shaul Mukamel</i>	691

Structures and Dynamics of Molecules on Liquid Beam Surfaces, <i>Tamotsu Kondow, Fumitaka Mafuné</i>	731
Effects of High Pressure on Molecules, <i>Russell J. Hemley</i>	763